# Characterization of Reflection Co-efficient for Ground-to-Aircraft and Satellite-to-Aircraft Communication Links

by

Abid Jamal

MEE143015

A thesis submitted to the
Department of Electrical Engineering
in partial fulfillment of the requirements for the degree of
MS. IN ELECTRICAL ENGINEERING

Faculty of Engineering
Capital University of Science and Technology
Islamabad

October 2016

*I dedicate this thesis to my brother Maqsood alam and to my loving parents for their love, endless support and encouragement.*

# CERTIFICATE OF APPROVAL

It is certified that the research work contained in this thesis has been carried out under the supervision of Dr. Noor M Khan, at Capital University of Science and Technology, Islamabad, Campus. It is fully adequate in scope and quality as a thesis for the degree of MS(EE) of Abid Jamal.

Supervisor:

————————————

Dr. Noor M Khan
Professor/HOD
Dep of Electrical Engineering
capital university of science and technology islamabad

Internal Examiner:

————————————

Dr. ——————-
Professor
Dept. of ——————-
Faculty of ——————-
University Name.

External Examiner:

————————————

Dr. ——————
Professor
Dept. of ——————
Institution Name,
University or Institution

Dean:

————————————

Dr. Imtiaz Ahmad Taj
Professor/Dean
Dept. of Electrical Engineering
Faculty of Engineering & Applied Sciences.
capital university of science and technology islamabad.

# ACKNOWLEDGMENT

# DECLARATION

It is declared that this is an original piece of my own work, except where otherwise acknowledged in text and references. This work has not been submitted in any form for another degree or diploma at any university or other institution for tertiary education and shall not be submitted by me in future for obtaining any degree from this or any other University or Institution

Abid Jamal

MEE143015

October 2016

# ABSTRACT

Because of high sensitivity and long range capability in modern radars, Radar Cross-Section (RCS) is to be considered one of the most important factors in the performance evaluation of stealth technology and for defense applications, especially those that deal with airborne weapon system. In this thesis, a concrete relationship is established between RCS and reflection coefficient for the two proposed scenarios, i.e. Ground-to-Aircraft and Satellite-to-Aircraft communication links. In this study, the world's largest commercial Aircraft A380 is selected as the target object. The 3D realistic model of the Aircraft A380 and its stereo-lithography (STL) file is develop in AutoCAD software. Geometrical models of the two proposed scenarios are used for the correct estimation of the incidence angles for the target aircraft. The well-established software tool developed by David C. Jenn, known as POFACETS is used for the correct estimation of the RCS. The obtained RCSs of A380 at different incident angles are used to find the reflection coefficients of the target aircraft. Factors that affect the behavior of RCS, i.e. orientation, incidence angles, and frequency have been studied and analyzed. Fluctuation on the gain or ratio of RCS major spike to minor spikes are deeply discussed. Various results of RCS is simulated in Matlab® against bistatic angles for both Ground-to-Aircraft and Satellite-to-Aircraft Communication Links.

# TABLE OF CONTENTS

# Chapter 2

# Chapter 3

# **Chapter** 4

# **Chapter** 5

# LIST OF FIGURES

# LIST OF TABLES

# LIST OF ACRONYMS

RCS      Radar Cross Section

RADAR   RAdio Detecting And Ranging

CW       Continuous wave

EM       Electromagnetic

PR       Pulse Radar

DR       Doppler Radar

dBsm    decibels square meter

LoS      Line of Sight

CAD     Computer-aided design

SL       Stereolithography

GUI     Graphical-user-interface

EIRP    Equivalent Isotropically Radiated Power

PO      Physical Optics

ILS      Instrument landing system

# LIST OF SYMBOLS

| Symbol | Description |
| --- | --- |
| $\sigma$ | Radar Cross Section |
| $T_x$ | Transmitter Antenna |
| $R_x$ | Receiver Antenna |
| $S_min$ | Minimum detectable signal |
| $D_t$ | Distance between target and transmitter |
| $D_r$ | Distance between target and receiver |
| $L_s$ | Losses due to system |
| $\varepsilon$ | Permittivity |
| $\mu$ | permeability |
| $\omega$ | angular frequency |
| $\theta_i$ | Incidence angle |
| $\theta$ | Bistatic angle |
| $\lvert\Gamma\rvert$ | Reflection coefficient |
| $\sigma_B$ | Bistatic RCS |
| $Z_o$ | Intrinsic impedance of the space |
| $K$ | Wave number |
| $(P_r)_{ref}$ | Power received from reflected path |

# Chapter 1

## INTRODUCTION

This chapter introduces the topic of Radar Cross Section (RCS) and discusses the factors that affect its behavior. Furthermore, this chapter also discusses the operation and types of RADAR and throws light on the reflection coefficient that affects signal reception at the receiving point.

## 1.1 Overview

A device for transmitting electromagnetic signals and receiving echoes from objects of interest within its volume of coverage is known as Radar. Nearness of an objective is uncovered by transponder reply or by the detection of its echo. Additional information about a target provided by a radar includes one or more of the following: direction, by use of directive antenna patterns; distance (range), by the elapsed time between transmission of the signal and reception of the returned signal; description or classification of target, by analysis of echoes and their variation with time; rate of change of range, by measurement of Doppler shift [2].

RCS is a measurement of an object's visibility towards the radar. Radar search continuously to detect an object. RCS of the object is directly proportional to the power received by the radar. Because of high sensitivity and long range capability in modern radars, RCS is to be considered one of the most important factors in the performance evaluation of stealth technology and for defense applications, especially those that deal with airborne weapon system. In the designing of modern fighter aircraft's, the performance of stealth technology and visibility of an aircraft is based on the results and measurements of RCS. In order to accurately predict RCS of a target, it is necessary to analyze the factors that affect its behavior, such as material, incident angle, radar signals wavelength, size of the target and

its orientation.

RCS is an important factor to consider in the design of many systems for modern warfare. Although the equations determining RCS are well understood, in practice predictions using numerical methods and measurements of both scale models and the full-size targets are required during the development of new systems. The processing power now becoming available has increased the scope of predictive computer codes and the diagnostic information available from measurements.

## 1.2    Research Objectives

As discussed earlier, RCS can be easily simulated and predicted by using well-established simulation tools with high processing capabilities. However, almost no work has been done on utilizing these simulated results for the characterizing of Reflection Coefficients, of concerned communication links. In our research work thus we intend to characterize Reflection Coefficients of an aircraft's surface for Radar Tx-to-aircraft and aircraft-to-Radar Rx links at various incident angles w.r.t aircraft's orientation. In this study, we assume two scenarios, i.e. Ground-to-Air and Satellite-to-Air Communication links.

## 1.3    RADAR

RADAR remains for RAdio Detecting And Ranging and as demonstrated by the name, it depends on the utilization of radio waves. Radars convey electromagnetic waves. The signs are conveyed as short pulses which might be reflected by target aircraft in their way, to a limited extent reflecting back to the radar. This idea is like listening to a reverberate. Albeit as of now designed, radar was further created amid World War II, with work on the innovation invigorated by the danger of air assaults. Radar had numerous utilization's amid the war-it was utilized for finding adversary boats and flying machine, to direct gunfire, and to help ship and flying machine navigation.

Modern radar's are now advanced and smart, it can be used for a wide array of applications.

Radar systems can be categorized by their features into the following subsets [3]:

•**Radar location:** fixed, mobile unit, space borne,ground and air-borne.

•**Capacity:** surveillance, tracking, imaging, reconnaissance

•**Applicability:** Military technology, meteorology, astronomy, transportation, Vehicle collision Avoidance, Air-traffic control, Satellite tracking, Border Air surveillance Radar and Assisted Mining.

## 1.3.1  Radar Range Equation

The scope of radar relates radar condition to the attributes of the beneficiary, the transmitter, the recieving wires, environment and the objective. To decide the most extreme conceivable range at which any radar can distinguish an objective, it is valuable to have some knowledge about the factors that affect the performance of radar [4]. A general overview of a radar geometry is shown in Fig. 1.1. The $T._X$. and $R._X$. blocks represent the transmitter and receiver antennas with the gain $G_t$ and $G_r$ respectively, while the target is located to the right side represented by an aircraft with an RCS, $\sigma m^2$. Target range is assumed to be equal to R, because receive and transmit antennas are placed close to each other.
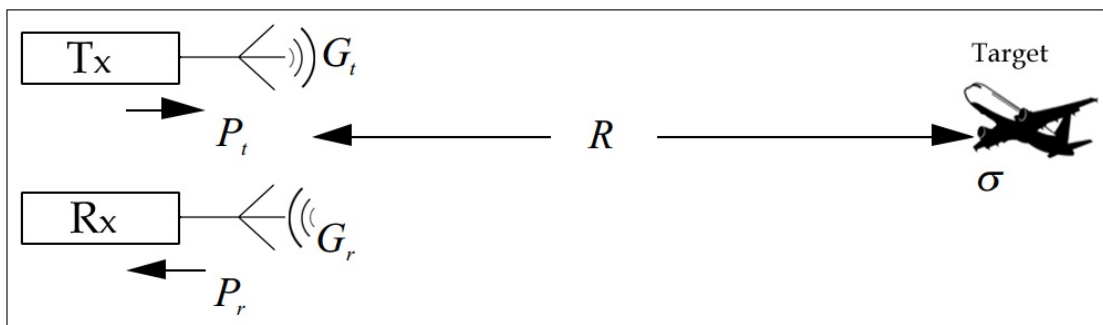


FIGURE 1.1: *Typical Radar−Target Scenario* .

The power received by the radar's receiver block Rx in watt is given as

$$P_r = \left(\frac{P_t G_t}{4\pi R^2}\right)\left(\frac{\sigma}{4\pi R^2}\right)\left(\frac{G_r \lambda^2}{4\pi}\right) \qquad Eq\ (1.1)$$

Where $P_t$ is the transmit power of Tx antenna block (in watts) and $\lambda$ is the wavelength of radar's signals.

Redar measuring power at the target is represented by the first term in parenthesis in *Eq (1.1)*. Scattering or reflection that occurs on the target represents the Redar measuring power at the receiving radar. It is equal to the product of the first and the second terms inside parenthesies. The measure of the reflected power determine by the getting radio signals gap is mentioned to by the third term in enclosure in *Eq (1.1)*.

## 1.3.2   Types of Radars

**Monostatic Radart**

When both transmitting and receiving antennas are placed closed to each other at the same location for the detection of an object is known as monostatic radar. There is only one radar, containing the same Tx and Rx antenna located on the ground for the detection of an aircraft's. The typical geometry of monostatic radar is shown in Fig. 1.2.

Transmitting and receiving Gain in the case of monostatic radar would be the same, and Gt and Gr must be equals to G = Gr = Gt, *Eq (1.1)* can be written as:

$$P_r = \frac{P_t G^2 \sigma \lambda^2}{(4\pi)^3 R^4} \qquad Eq\ (1.2)$$

The highest distance range of a given radar, Radarmax, is the length behind that the object can't be recognized. It happens when the got flag control $P_{.r}$ just equivalents the base discernible signals $S_{\min}$ [4] . By rearranging terms and substitute $S_{\min} = P_r$ in *Eq (1.2)* gives:
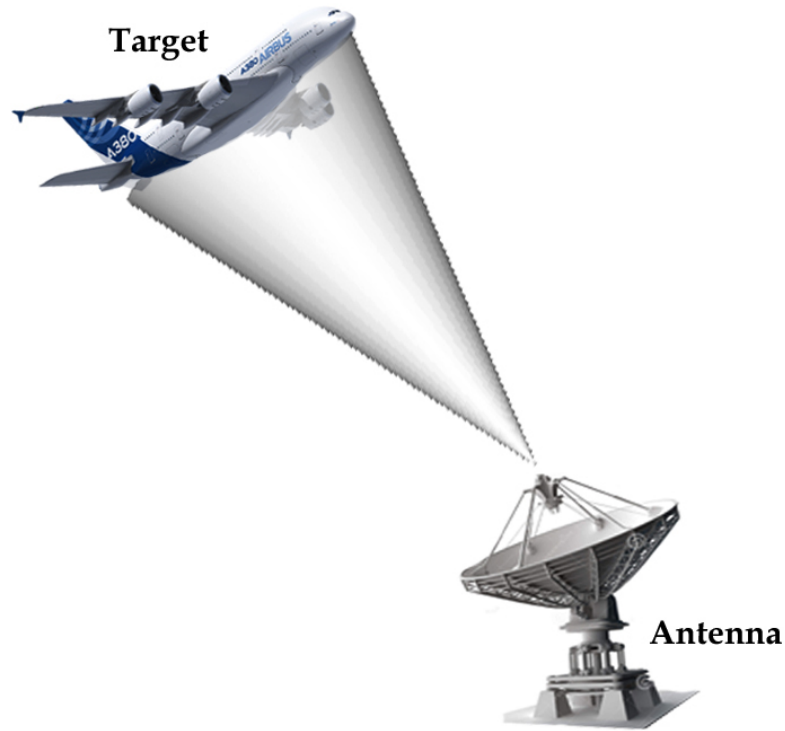
FIGURE 1.2: *A typical Monostatic radar.*

$$R_{\max} = \left[\frac{P_t G^2 \sigma \lambda^2}{(4\pi)^3 S_{\min}}\right]^{1/4} \qquad\qquad Eq\ (1.3)$$

Despite the fact that this type of the radar condition avoids numerous vital elements and for the most part predicts high values for greatest range, it portrays the relationship between the greatest radar go and the objective's RCS.

**Bistatic Radar**

When both transmitting and receiving antennas are placed apart from each other at some considerable distance is called bistatic radar. A system at which there is one transmitter and multiple separated receivers is known as multistatic radar. The geometry of bistatic radar is shown in Fig. 1.3. If $\alpha$ the bistatic angle, is small then bistatic RCS is similar to that of monostatic RCS.
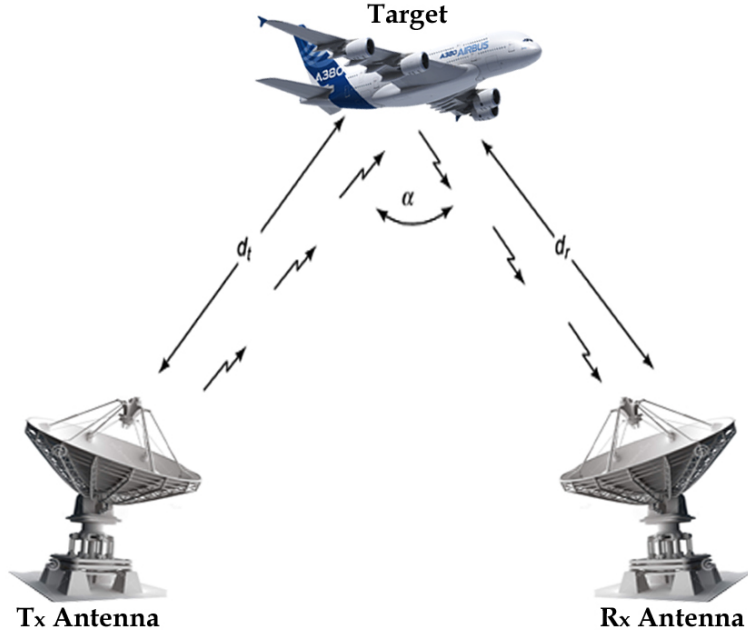
FIGURE 1.3: *Geometry of bistatic radar.*

Bistatic Radar Equation [5]

$$P_r = \frac{P_t G_t G_r \lambda^2 \sigma_b}{(4\pi)^3 D_t^2 D_r^2 \mathrm{L_{p,t}} \mathrm{L_{p,r}} L_s} \qquad\qquad Eq\ (1.4\,)$$

Where, $\sigma$ is the bistatic radar cross section (in $m^2$ ), $D_t$ the distance between target and transmitter , $D_r$ the distance between target and receiver , $\mathrm{L_{p,t}}$ the target to transmitter path propagation loss , $\mathrm{L_{p,r}}$ the target to receiver path propagation loss , and $L_s$ the losses due to system .

**Continuous wave (CW) radar**

CW radar can transmit Electromagnetic waves (EM) all the time, with 100% duty cycle for the detection of an object. CW radar use less amount of power for the working operation as compared to other radar's. CW radar can measures velocity from Doppler shift. Conventional CW radar cannot measure range because there is no basis for the measurement of the time delay [6].

**Pulse Radar (PR)**

PR has an ability, to transmit EM waves in the form of pulses or bursts to measure velocity and range of a target. PR uses amplitude modulation. PR can calculate the time interval between received and transmitted pulses to measure the target range.The PR is used determine direction and distance of the target.

**Doppler radar (DR)**

DR is a specialized radar and it can produce radial velocity data to measure the Doppler effect about the objects. When the object is in motion, it can cause fluctuation in returned signal frequency. With the help of DR we can measure the movement of the target, that it is going either away or toward from the radar. Doppler radars are used in meteorology, risk assessment, aviation, nursing and health care. Mostly DR is used to measure the speed and direction of the wind.

## 1.4    Radar Cross Section

RCS is an estimation of how much power is scattered or reflected back towards the direction of the receiver antenna, when target is illuminated by an incident wave [7]. Incident energy of an EM wave disperses in all directions when it is impinged on rough surfaces. The surface on which the energy of EM wave is dispersed is known as scatterer, while the phenomenon is called as scattering.

RCS can be defined as [8, 9],

$$\sigma \equiv 4\pi . \frac{P_s}{P_i} \qquad\qquad Eq\ (1.5)$$

$$\sigma \equiv 4\pi . \frac{\text{Power refleced to receiver per unit solid angle}}{\text{Power density,or intensity,of a plane wave striking the target}}$$

In description of the incidence and scattered fields, there is another sophisticated way to write the RCS as [10]:
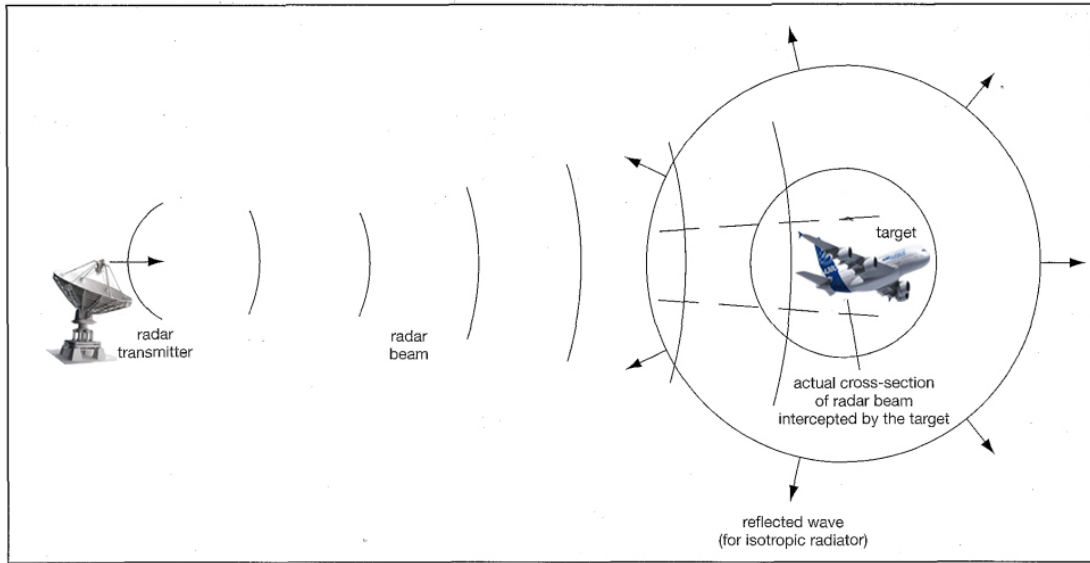
FIGURE 1.4: *Isotropical Distribution of energy in all directions.*

$$\sigma = \lim_{R\to\infty} 4\pi R^2 \frac{|E_s|^2}{|E_i|^2} \qquad\qquad Eq\ (1.6)$$

As we know R is the possible length between the object and the transmitting source also knows as illuminating device, and $E._i$ and $E._s$ the electrics field peaks of the incidence and reflected field, separatley. In equation *Eq (1.6)*, it,s assumed that distributions of energy is uniformed in all directions. Target is far enough from the radar, so it,s to be condisdered that the movement of electric field of the incidence wave can be defined is to be in planar, not other than spheriecal. The derivation assumes, but in practicle all the targets do not scatter energy in all the directions uniformly. The Power density of the incident field is normalized (1/R), to remove the effect of the range and make RCS independent of the distance [5, 11].

### 1.4.1 Significance of the RCS

RCS ranges are used to test the radar signatures of various objects. Essential pursuit radars might be constrained in affectability, since they are required to

check an expansive strong point in a brief span, and unavoidable exchange offs are required amongst affectability and coverage.The utilization of a slender shaft gives high pick up and will allow the radar to identify a little target, however it might set aside a long opportunity to cover the required sweep range. Typically more extensive bars are utilized for target searches,resulting as a part of lower pick up and decreased affectability. The course, speed and maybe even personality of an objective can be resolved from its radar mark, and it can be followed and its future position anticipated. To make a critical mission successful against enemy, RCS minimization of fighter aircraft is an important factor. Sometimes minimization of RCS may cause and enlist other countermeasures, such as jamming. RCS is to be considered the most important parameter, even after detection of target. Enemy uses different techniques to confuse the search radar. One of the most common techniques is known as chaff, in which aircraft release small pieces of aluminum in free space to disturb the tracking capability of search radar. Effectiveness of defensive measures increases as they received a low RCS of a target. For large range of a systems and have confidence in successful operation it is essential to know the parameters, which affecting the RCS results. As radar frameworks keep on becoming more touchy and smarter,so there is a proceeding with drive to see more unpretentious RCS instruments and to diminish the RCS of our stages considerably further

### 1.4.2   Unit of RCS, dBsm

In *Eq (1.5)*, the unit of the denominator is Watts/$m^2$ while the unit of the numerator is Watts. Thus the unit of RCS becomes $m^2$, but most commonly, it is used in decibels square meter (dBsm). Logarithmic (decibel) power scale is most oftenly used to cover large dynamic range of the RCS.

$$\sigma[\text{dBsm}] = 10\log(\sigma[\text{m}^2]).$$
*Eq (1.7)*

### 1.4.3 Factors that affect RCS

**Size of the target**

The size of a target as seen by radar is not always related to the physical size of the object.If the size of the target is large, then it has a strong reflection capability and will change the behavior of the RCS as compared to others target with normal size. The absolute and real size of a target is very important factors in the study of RCS

TABLE 1.1: Typical RCS Values [1]

| Objects | $\sigma(\mathbf{m^2})$ | $\sigma$ (dBsm) |
|---|---|---|
| Ships A/C carriers | 10000- 100000 | 40-50 |
| Bomber Aircraft | 1000 | 30 |
| Fighter Aircraft | 100 | 20 |
| Tank | 10 | 1 |
| Human being | 1 | 0 |
| Guns | 0.1 | -10 |
| Birds | 0.01 | -20 |
| Insects | 0.001 | -30 |

**Incident angle, orientation and geometry of the object**

The measure of RCS highly depends on the reflected amount of EM wave energy back to the source which is highly influenced by three factors: incident angle of EM waves, orientation and geometry of the object. The value of RCS fluctuates when a particular portion of the target object is hit by radar waves at different incident angles. These angles basically give direction to the reflected waves which in result when received at the receiver gives the measure of the RCS. The orientation of the object relative to the radar is very important for strong RCS because this depends on how RADAR eye look an object. A plane will present larger RCS when viewed from the side as compared to front view. Thus, the RCS measure would be different for different orientations of the object and need a closer look to identify it. Finally, the geometry of the object which is the most important factor for the measurement of RCS. The geometry of the object can be designed

to by-pass the EM waves. Sometimes, it becomes hard to predict and measure RCS of a target with complex geometry like in Stealth aircrafts which are designed to reflect the signal somewhere else other than towards the source.

**Polarization of an incident wave**

Polarization is one important factor which often affects the results of RCS. This is because the sensing of RADAR receiving antenna is based on the concept of antenna theory in which the polarization effects are very important for transmission and reception of EM waves. Thus, the effect of polarization could be severe in the measurements of RCS. A target can hide himself from the RADAR eye by depolarizing the incident waves. This is because, the RADAR receiving antenna would not be able to sense reflected EM waves and hence, the target would become invisible to it.

**Material**

Materials such as metal and aluminum are strongly radar reflective and tend to produce strong signals. There are some materials which produce low reflectivity, such as fiberglass, plastic, wood and cloth. There must be a difference between the RCS results for the two different materials like metal and plastic.

**Frequency and wavelength**

The RCS conduct changes as indicated by the connection between the wavelength and the objective size. As such, the RCS reaction of an objective relies on upon the RADAR's wavelength. At the point when the objective size is littler than the wavelength utilized, the objective goes about as a point source and the RCS esteem is so little for this circumstance. On the off chance that the wavelength is about equivalent to the objective size, the objective adds to the RCS examination all in all with every one of its edges. For the circumstance that the wavelength is littler than the objective size, the parts of the objective can be inspected independently in detail.

## 1.5 Reflection Coefficient

Reflection coefficient is the ratio of the amplitude of the incident wave to the reflected wave. Reflected wave can be characterized by knowing polarization, electrical properties of the medium and the incidence angle of the transmitted signal. The perpendicular and parallel reflection coefficients are usually denoted by $\Gamma_\perp$ and $\Gamma_\parallel$ respectively. Both reflection coefficients involve path properties such as transmitted angle ($\theta_t$), incidence angle ($\theta_i$), refraction index (n) and Intrinsic impedance ($\eta$) and can be given as [12].

$$\Gamma_\parallel = \frac{E_r}{E_i} = \frac{\eta_2 \cos\theta_t - \eta_1 \cos\theta_i}{\eta_2 \cos\theta_t + \eta_1 \cos\theta_i} \qquad\qquad Eq\ (1.8)$$

$$\Gamma_\perp = \frac{E_r}{E_i} = \frac{\eta_2 \cos\theta_i - \eta_1 \cos\theta_t}{\eta_2 \cos\theta_i + \eta_1 cos\theta_t} \qquad\qquad Eq\ (1.9)$$

Parameters that define the characteristics of a general medium, include permittivity ($\varepsilon$), permeability ($\mu$), angular frequency ($\omega$) and conductivity ($\gamma$). Intrinsic impedance ($\eta$) can thus be written as,

$$\eta = \sqrt{\frac{j\omega\mu}{\gamma + j\omega\varepsilon}} \qquad\qquad Eq\ (1.10)$$

The decomposition of an incident E-field or reflected E-field into two parts, *i.e.* parallel and perpendicular components is shown in Fig. 1.5

On account of opposite polarization, Ei, is opposite to the plane of occurrence, the plane containing the bearing of engendering of the occurrence wave and the typical to the limit surface. For the situation of parallel polarization, Ei is parallel to the plane of frequency. The parallel reflection coefficient is demonstrated as $\Gamma_\parallel$. Parallel polarization is additionally alluded as vertical polarization or H-polarization. Reflection coefficients are mind boggling amounts that speak to the
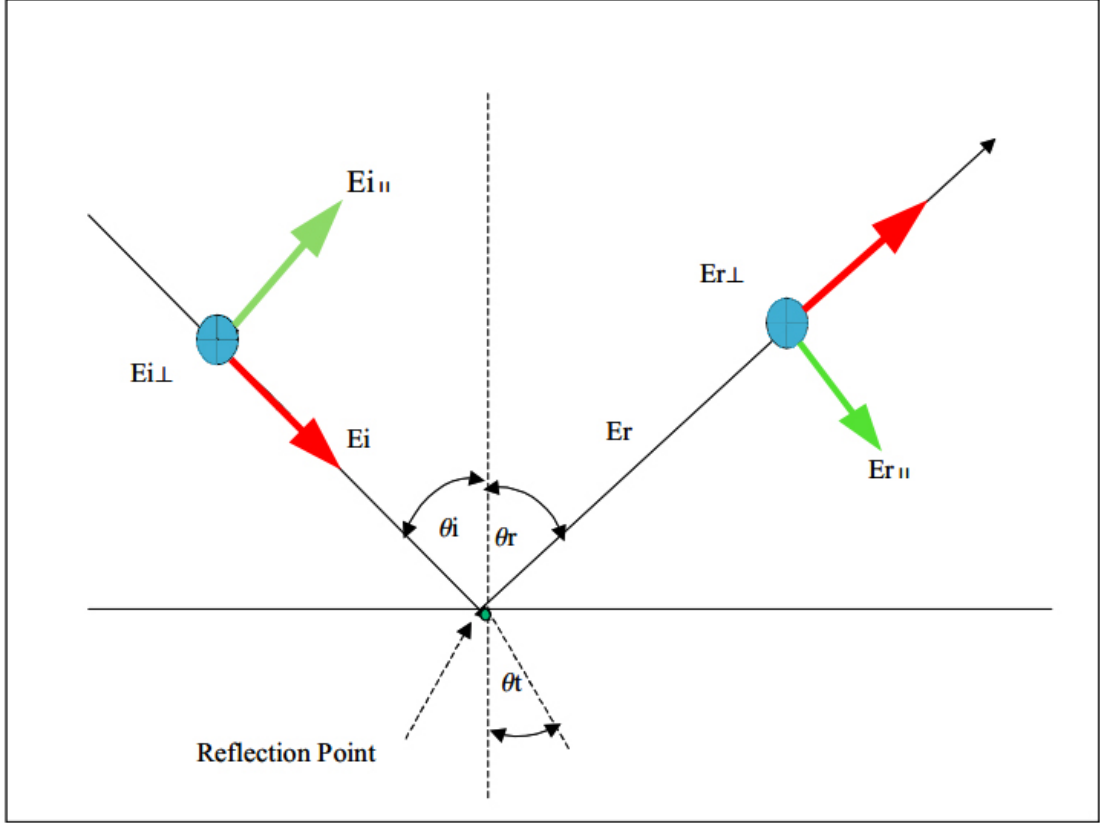
FIGURE 1.5: *Reflected and incident E-field .*

extent and stage change of the E-field segments at the interface medium. These progressions are in charge of depolarization.

From the above conditions, with the expectation of complimentary space $\eta_1 = \eta_0 = 120\pi$, refraction file, $n_1 = 1$, and $n_1/n_{\cdot 2} = \eta_{2\cdot}/\eta_{\cdot 1}$. Along these lines, the reflection coefficients can be communicated as:

$$\Gamma_{\cdot\parallel} = \frac{E_r}{E_i} = \frac{\sqrt{n_{\cdot}2^2 - \sin^2\theta_i} - n_2^2\cos\theta_i}{\sqrt{n_2^2 - \sin^2\theta_i} + n_2^2\cos\theta_i} \qquad\qquad Eq\ (1.11)$$

$$\Gamma_{\cdot\perp} = \frac{E_r}{E_{\cdot i}} = \frac{\cos\pi_i - \sqrt{n_2^2 - \sin^2\theta_i}}{\cos\theta_i + \sqrt{n_2^2\sin^2\theta_{\cdot i}}} \qquad\qquad Eq\ (1.12)$$

13

## 1.5.1 Reflection coefficient in the case of Two Ray Model

The two beam model is generally used to speak to ground reflection wonders in the radio channel.The demonstrate contains, reflected electric field E-field and an immediate Line of Sight (LoS) E-field as appeared in Fig. 1.6.
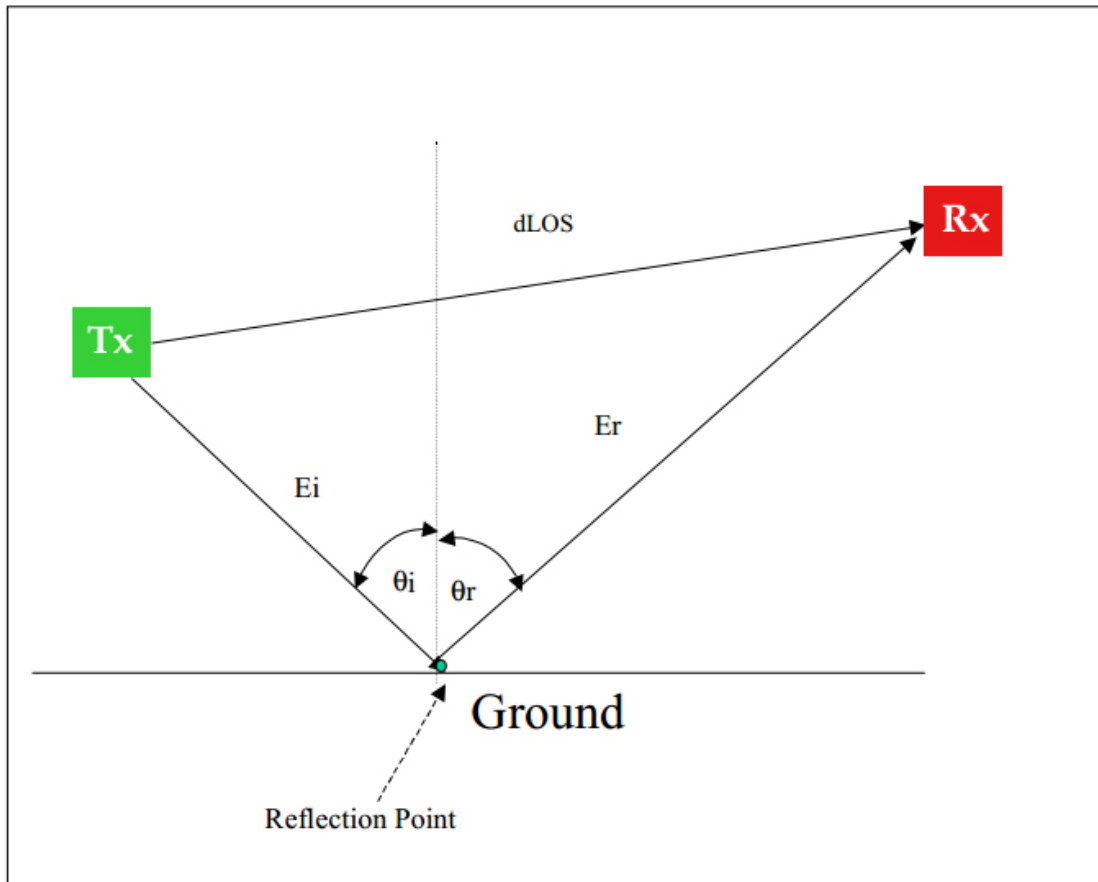


FIGURE 1.6: *Two ray model (Ground Reflection) .*

If a two ray ground reflection model is pretended, the total E-field received will be the sum of the LoS E-field and the E-field of the ground reflected component:

$$E_{\cdot\text{totel}} = E_{\cdot\text{los}} + E_{y} \qquad\qquad Eq\ (1.13)$$

The complex reflection coefficients for perpendicular polarization is expressed as [13]:

$$\Gamma_\perp = \frac{\cos\theta - \sqrt{(\varepsilon_r - \mathrm{jx}) - \sin^3\theta}}{\sin\theta. + \sqrt{(\varepsilon_u - \mathrm{jxs}) - \cos^3\theta}} \qquad Eq\ (1.14)$$

angle for the incidence $\theta$ is defined as from ground to the plane of the incedense wave. The distracted reflection coefficient, For polarization-parallel is given as:

$$\Gamma_\parallel = \frac{(\varepsilon_r u - \mathrm{jxs})\sin\sin - \sqrt{(\varepsilon_r u - \mathrm{jx}) - \cos^3\theta}}{(\varepsilon_r - \mathrm{jx})\sin\theta + \sqrt{(\varepsilon_r u - \mathrm{jx.}) - \cos^3\theta.}} \qquad Eq\ (1.15)$$

Where $\gamma$. is the conductivity of the medium (in Simens/meter), $\varepsilon_r$ is the relative dielectric constant related to polarization and anomalous dispersion, while the imaginary part jx is associated with dissipation of energy into the medium. The reflection coefficient for both parallel and perpendicular polarization tends to -1 for grazing incidence angle ($90^o$), along these lines stage and the solidarity plentifulness are switched and the contrast between the two polarization has a tendency to be little to the extent reflection from the smooth ground is concerned[13].

## 1.5.2   Relationship of received power and electric field

With parameters such as range, signaling frequency, transmitter hight and receiver antennas hights above the ground, received E-field, gain and effective aperture of the receiver antenna, the received power can be obtained [14].

$$P_r(d) = P_d A_e = \frac{|E|^2}{120\pi} A_e = \frac{|E|^2}{120\pi} \frac{G_r \lambda^2}{4\pi} = \frac{P_t G_t G_r \lambda^2}{(4\pi.)^2 d^2} \qquad Eq\ (1.16)$$

where, in free space $P_d$. is the density for power flux, $d$. is the total equilaent distacne $(d_{los} + d_{ref})$ what's more, $E$. is the aggregate got electric field, which may incorporate both reflected and LoS E-field. This condition is known as the Friis transmission condition, and is fundamental in any radio connection, to figure got control effortlessly [15]. The LoS control from the normal LoS defer profile was

15

taken to be the free space esteem:

$$(P_r)_{\text{Los}} = \frac{P_t G_t G_r \lambda^2}{(4\pi d_{\text{Los}})^2} \qquad\qquad Eq\ (1.17)$$

The averaged reflected power delay profile for the reflected path measurement was calculated as [16, 17],

$$(P_r)_{\text{ref}} = \frac{P_t G_t G_r \lambda^2}{(4\pi)^2 (d_1 + d_2)^2} |\Gamma|^2 \qquad\qquad Eq\ (1.18)$$

Incident wave striking the surface could be approximated as a plane waves for transmitter distance $(d_1)$. Solving $Eq\ (1.18)$, for the empirical reflection coefficient yields

$$|\Gamma| = \frac{d_1 + d_2}{d_{\text{Los}}} \sqrt{\frac{(P_r)_{\text{ref}}}{(P_r)_{\text{los}}}} \qquad\qquad Eq\ (1.19)$$

So after simplifying, $Eq\ (1.19)$ becomes:

$$(P_r)_{\text{ref}} = \frac{d_{\text{Los}}^2}{(d_1 + d_2)^2} (P_r)_{\text{Los}} |\Gamma|^2 \qquad\qquad Eq\ (1.20)$$

The point target radar range equation estimates the power at the input to the receiver for a target of a given RCS at a specified range. The equation for the power at the input to the receiver was calculated as [18],

$$(P_r)_{\text{ref}} = \frac{P_t G_t G_r \lambda^2 \sigma_{\text{B}}}{(4\pi)^3 d_1^2 d_2^2} \qquad\qquad Eq\ (1.21)$$

Where, $\sigma_B$ is the bistatic RCS (in $m^2$ ), $d_1$ the distance between target and transmitter, $d_2$ the distance between target and receiver. To derive our own formula

for the Reflection Coefficient, we put $(P_r)_{\text{ref}}$ value in *Eq (1.20)*, we get:

$$
\begin{aligned}
\frac{d_{\text{Los}}^2}{(d_1 + d_2)^2}(P_r)_{\text{Los}}|\Gamma|^2 &= \frac{P_t G_t G_r \lambda^2 \sigma_{\text{B}}}{(4\pi)^3 d_1^2 d_2^2} \\
|\Gamma|^2 &= \frac{P_t G_t G_r \lambda^2 \sigma_{\text{B}}}{(4\pi)^3 d_1^2 d_2^2} \frac{(d_1 + d_2)^2}{d_{\text{Los}}^2} \frac{1}{(P_r)_{\text{los}}} \\
|\Gamma|^2 &= \frac{\sigma_{\text{B}}(d_1 + d_2)^2}{(4\pi) d_1^2 d_2^2} \\
|\Gamma| &= \frac{(d_1 + d_2)}{d_1 d_2} \sqrt{\frac{\sigma_{\text{B}}}{4\pi}} \qquad\qquad Eq\ (1.22)
\end{aligned}
$$

Final look of the Reflection Coefficient formula is indicated in *Eq (1.22)*, we derived this formula with the help of different equations. Later on Chapter 4 we will use this formula to find our results on the basis of Reflection Coefficient. Target
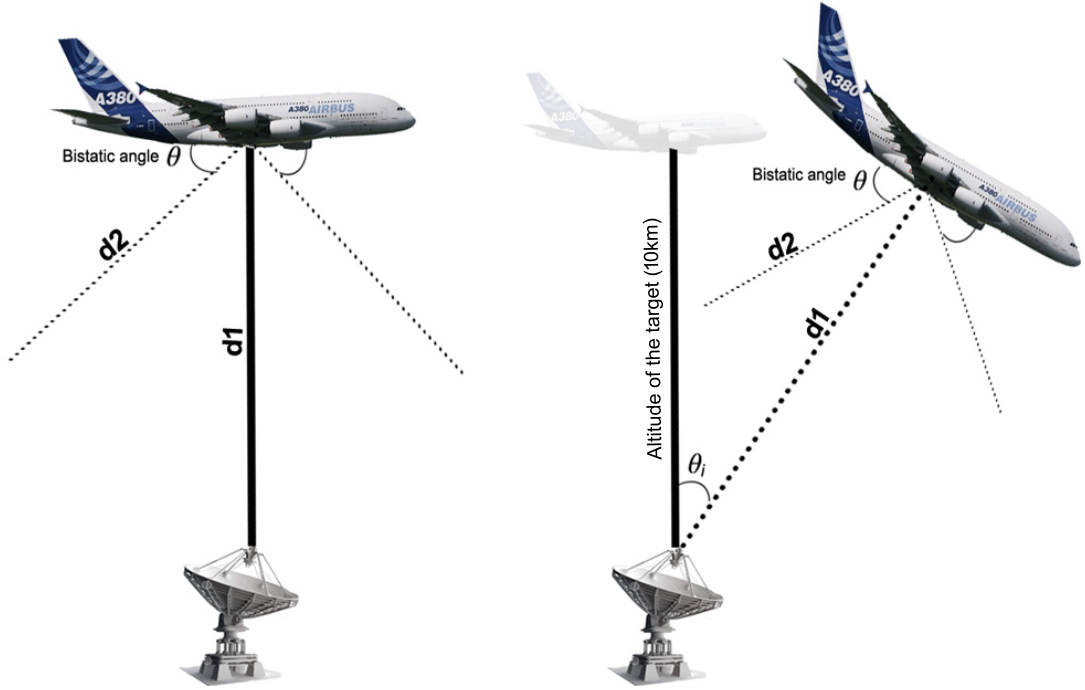


FIGURE 1.7: *Geometrical model for the disctances $d_1$ and $d_2$*

Aircraft A380 is flying above the ground with an altitude of 10km as depicted in Fig. 1.7. If we know the incidence angle $\theta_i$, then we can easily find the distance $d_1$

covered by the aircraft from its initial position by applying a cosine rule. Distance $d_2$ is dependent on bistaic angle. Later on Chapter 4, by applying a cosine rule we will find out the distances $d_1$ and $d_2$ with the help of incidence angle $\theta_i$ and bistatic angle $\theta$ respectively.

## 1.6    Thesis organization

The rest of thesis is organized into four chapters. Chapter 2 presents the literature survey of the proposed research and states the problem formulation and methodology to solve this problem. Chapter 3 presents the system models of the two proposed scenarios, *i.e.* Ground-to-Air and Satellite-to-Air communication links. It describes the AutoCAD based designing of the objects and their RCS acquisition. Chapter 4 focuses on the simulation results and discussions. A detailed discussion on RCS and Reflection Coefficient related to an Aircraft is also made in this chapter. Chapter 5 concludes the thesis and discusses its future work.

# Chapter 2

## LITERATURE SURVEY AND PROBLEM FORMULATION

This chapter gives a brief overview of the literature survey in its section 2.1. In section 2.2, the description of the different methods for the prediction of RCS is presented. In the end, section 2.6 and 2.7 present the problem formulation and research methodology.

## 2.1 Literature Survey

Because of recent advances in high-frequency circuit technologies and data analysis, high precision measurements have become possible for RCS analyses using high frequency EM waves. One of the fundamental quantities for radar-related measurements is the radar RCS, which is the equivalent cross section of the scattering target, and depends on its shape [19, 20].

On radar systems, RCS is mostly used for detection purposes. It introduces spatial RCS fluctuations using Physical Optics (PO) method to address a tradeoff between computational cost and accuracy. For accurate RCS interpolations, it was found that spline approximations provide good results as compared to bilinear interpolation [21]. Although this work is limited; however, the data generated with the Physical Optics (PO) to interpolate RCS was only for a single object.

In the literature, experimental apparatus has been used to measure the backscattered RCS for a full sized engine cavity structure. RCS was measured from this generic aircraft engine inlet with a fan assembly. The details of these experimental measurements and characterization of the RCS are available in [22]. However, to improve the RCS results a realistic engine cavity model would be required.

To increase the performance and the computational speed, authors of [23, 24] proposed the concept of using interpolation for the measurement of RCS. In this work, RCS was uses as interpolant and the azimuth and elevation angles were the interpolation variables for the investigation of bivariate interpolation.

Statistics of aircraft RCS are estimated in [25]. It was found that the fluctuations of RCS with aspect angle were considerable. It was noted that to obtain a reliable result, the spatial RCS variations must be addressed in simulation and modeling.

In the literature, the authors of [26] investigated and found that the performance of the directional pattern of the instrument landing system (ILS) and the localizer antenna system can be disturbed by reflections from large aircrafts on the ground. For measurement purpose, scale models of A380 and B747 were considered. The orientation of the aircraft on the ground was taken perpendicular to the runway. Their bistatic RCS results have been measured and it was found that the A380 tends to have a slightly larger disturbing influence as compared to B747. However, it is needed to measure the bistatic RCS of disturbing aircraft for more orientations and positions.

A quasi-monostatic technique with monostatic calibration has been proposed in [27] for the measurement of the RCS of conducting plate and parallel plate in a relatively small anechoic chamber. Data processing was effectively applied to eliminate background noise such as the isolation error of the antenna setting, reflected waves from the back wall of the chamber. It was concluded that the quasi-monostatic configuration have a wider dynamic measurement range and more stable measurement data than the monostatic one. However, these measurements are done at 10 GHz lower frequency, for further refinement it is necessary to analyze the behavior of RCS for higher frequency $> 10$ GHz range.

In the literature, the authors of [28] proposed a conceptual design of the shipborne early warning aircraft. For the designing purposes, CATIA software was used to

make a successful 3D model of the aircraft. Physical optics method and the equivalent electromagnetic bow method were used to simulate the RCS characteristics. It was found that bistatic RCS of the design of the shipborne early warning aircraft were reduced to 39.26 %. The results were then compared with foreign advanced aircraft, and it was concluded that RCS characteristic of the conceptual design is better under any band and azimuth.

To evaluate the effectiveness of scattering, first of all simple shapes such as an equilateral triangle, circular cylinder and square cylinder were considered in [29]. Furthermore, the authors of [29] used Aircraft model composed of basic shapes and examined their RCS behavior in optical, Mie, and Rayleigh regions using FDTD simulation at different frequencies. It was concluded that the frequency and geometry of the target are the two factors which affect RCS behavior.

Innovative approach has been proposed in [30] by using physical optics (PO) approximation to measure RCS and its analytical expression for perfectly random rough surfaces with its specifically geometric properties. It was found, that the computational speed of the numerical PO technique has been increased.

In the literature, the authors of [31] investigated the RCS of typical vehicles and pedestrian at anechoic chamber room for the two different frequencies (26GHz and 79GHz). It was concluded that the RCS of the flat parts, such as the front, side and rear for each vehicle, at 79GHz is approximately 10dBsm larger compared to that at 26GHz. It was found that the RCS for each target has a unique RCS pattern.

The physical Optics method has been proposed in [32] to predict the RCS of fuel tank of F16 fighter aircraft. The model of the fuel tank was made with the help of triangular meshes. It was found that the RCS of any object modeled by triangles can be calculated by using PO method. However, this work is not applicable to the object with large size and complex geometry.

In order to maximize predictive power of RCS, two techniques have been investigated in the literature [33] such as physical optics (PO) and the geometrical theory of diffraction (GTD). The authors also discuss means of integrating local scattering theories to analyze the RCS of large and complex targets. New Computer system has been developed for the RCS prediction of military platforms.

## 2.2 Different methods for the prediction of RCS

Some of the most common numerical RCS prediction methods for any 3D objects are the Geometrical Optics, Finite Difference Method, Method of Moments and Physical Optics. But among all of them Physical Optics (PO) method is commonly used for the prediction of RCS.

### 2.2.1 Method of Moments (MOM)

When target surface is broken into small number of pieces and to solve its integral equation is known is a method of moments. To obtain the integral equations for a target, MOM use boundary condition and Maxwells equations respectively. The complex and difficult step is to solve and reduce these integral equations. For the solution of integral equations, linear equations and standard matrix algebra are commonly used. However, this method fails to predict the RCS accurately in practical, if the size of the target is large and the wavelength of the signal is small. Furthermore, it requires high processing speed to solve large matrices [11, 8].

### 2.2.2 Microwave Optics (MO)

MO technique deals with those objects, which has a large size and arbitrary shapes. MO uses Rays tracing methods for the prediction of the RCS. Geometrical theory of Diffraction and Geometrical Optics are based on ray tracing methods. The working principle of ray tracing is simple, first object is bombarded with light. The object will disperse the light in different directions (i.e., reflect, diffract and

scatter) other than the desired, if it has a rough surface. Ray tracing is a technique to trace a light paths. The ray tracing method fails to predict the reflected light paths accurately for those objects which have a large size with complex geometry.

### 2.2.3    Finite Difference Methods (FDM)

The working principle of this method as same like MOM, but it can predict the target RCS by using Fourier transform. The Wavelength size must be greater than the small sub domains and this is the reason, it takes a large amount of time to execute the orders of the magnitude of the wavelength.

### 2.2.4    Physical Optics (PO)

The Physical Optics (PO) technique evaluates the surface current prompted on a subjective body by the occurrence radiation. On the bits of the body that are specifically enlightened by the episode field, the initiated current is essentially relative to the occurrence attractive field power. On the shadowed bit of the objective, the current is set to zero. The current is then utilized as a part of the radiation integrals to figure the scattered field a long way from the objective. PO is a high-recurrence estimation strategy that gives best results for electrically huge bodies ($L \geq 10\lambda$). It is most precise in the specular course.

## 2.3    Scattering Regions

As talked about before, the RCS relies on upon the recurrence of the occurrence wave. The scrambling attributes of an objective are subject to the recurrence of the episode wave. There are three recurrence areas in which the RCS of an objective is unmistakably extraordinary. The districts are characterized in view of the measure of the objective as far as the episode wavelength. For a smooth focus of length L, the meanings of the three recurrence administrations take after.

### 2.3.1 Low Frequency Region or Rayleigh Region

The first is the low Frequency locale or Rayleigh district $(\lambda >> L)$ where the stage variety of the episode plane wave over the objective is little $\left(\frac{2\pi}{\lambda}L << 1\right)$. Because of the little size of the objective, the state of the body is not critical for this situation. Accordingly, the actuated current on the body of the objective is roughly consistent in adequacy and stage.

### 2.3.2 Resonance Region or Mie Region

The second area is the reverberation district or Mie locale $(\lambda == L)$ where the stage variety of the current over the body is noteworthy $\left(\frac{2\pi}{\lambda}L \approx 1\right)$ and all parts add to the dissipating design. In this area the span of the objective must be equivalent to a size of a wavelength.

### 2.3.3 High Frequency Region or Optical Region

For these frequencies, there are numerous cycles in the stage variety of the current over the objective body and, subsequently, the scattered field will be extremely point subordinate. The size of the target must be greater then the size of a wavelength $(\lambda << L)$ for the case of optical region. In this study we use Optical Region as a scatter region. The reason for chosing the Optical Region is the large body size of the target(Aircraft A380).

## 2.4 Radiation Integrals for far zone Scattered Fields

The disseminating from a triangular aspect is an exceptional instance of the dissipating from a subjective body. Consequently, the recipe for the scattered field for a triangular aspect will be gotten from the one acquired for a discretionary body. Consider the circumstance portrayed in Figure 2.1. A discretionary disseminating

body is set at the root, with the perception point being at directions $(x., y., z.)$. For RCS calculations, the determination location is considered to be in the most
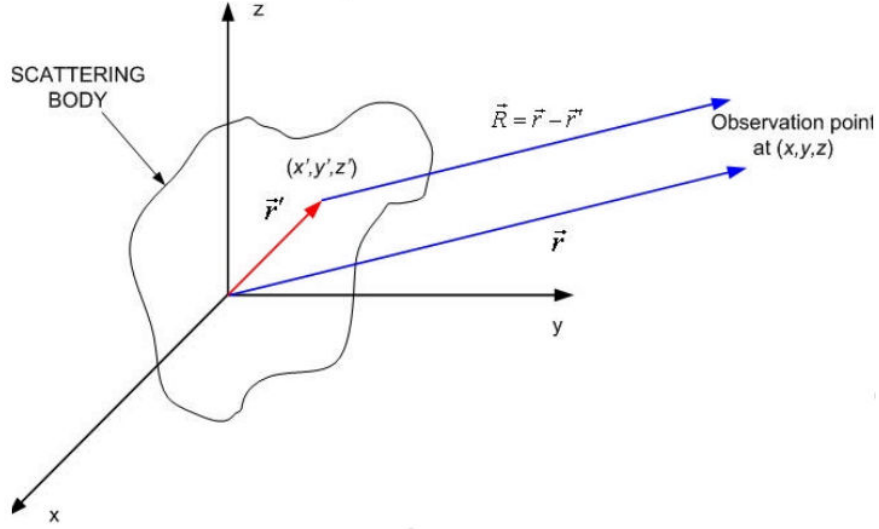


FIGURE 2.1: *Far Field Scattering from an Arbitrary Body.*

distant zone of the objective. In this manner, the vectors $\vec{R}u$ and $g\vec{r}$. are around parallel.

The body is portioned into limitlessly little source purposes of volume $v'$ situated at directions $(x', y', z')$ . The position vector to a source point is:

$$\vec{ru}' = \hat{x}.x.' + \hat{y}.y.' + \hat{z}.z' \qquad\qquad Eq\ (2.1)$$

with $\hat{x}., \hat{y}, .\hat{z}$ being the coordinates axes unit vectors. The unit vector toward the perception point is:

$$\hat{ru} = \hat{x}.u. + \hat{y}.v + \hat{z}.w \qquad\qquad Eq\ (2.2)$$

where

$$j = \sin .\theta \cos \phi$$

$$k = \sin .\theta \sin \phi \qquad\qquad Eq\ (2.3)$$

$$l = \cos .\theta$$

with $\theta$, and $\phi$, being of the observation points for the spherical cordinates. Expecting that the attractive volume current in the body is $\vec{Js}_m = 0$, the scattered field from the body is given by the accompanying condition [34]:

$$\vec{E}_s.(r, \theta., \phi) = E._\theta(r, phi, \phi.)\hat{\theta} + E_\theta(ru, \theta, \phi)\hat{\theta} = \frac{+jKy_o}{4\pi r}e^{+jkr}\iiint_V r\vec{Js}e^{jyx}yv.'$$

$$Eq\ (2.4)$$

where $\vec{J.s}$ is the curent of volume for electric field, $y_o$ is the inborn impedance of the space encompassing the body, $y = 2\pi./\lambda$ (with $\lambda$ being the wavelength) and g is characterized as:

$$g_s = r\vec{u}',dotr\hat{u} = x.'j + y.'k + z'l \qquad Eq\ (2.5)$$

as we look back again in to $Eq\ (2.4)$, the electric field has parts just in the $\theta$ and $\phi$ heading, so that the $E_r$ segment in $Eq\ (1.4)$ is overlooked [35].

## 2.5 Physical Optics Surface Current Computation

As indicated by the Physical Optics strategy, on the bits of the objective body that are specifically lit up by the occurrence field, the actuated current is basically relative to the episode attractive field power [34]. On the shadowed bit of the objective, the current is set to zero. Thus:

$$\vec{J}_s = \begin{cases} 2\hat{n} \times \vec{H_i}x & \text{for the facets which illuminated} \\ 0 & \text{for the facets which shadowed} \end{cases} \qquad Eq\ (2.6)$$

where $\vec{H}_i$ is the ration of the magnetic field for the incedence signals on the surface. In common, the form of incidence field as

$$\vec{E}_i = (E_{i\theta}\hat{\theta} + E._{i\phi}\hat{\phi})e^{-j\vec{k.}_i\bullet\vec{r}} \qquad Eq\ (2.7)$$

where $\vec{k}_i = k\hat{k}_i = -kr\hat{u}_i$, with $y = 2\pi/\lambda$.. Thus $\hat{r_p} = \hat{r}$ point is for $(J_p, K_p, L_p)$ in the surface,

$$\vec{E}_i = (E_{i\theta}\hat{\theta} + E_{i\phi}\hat{\phi})e^{jk\hat{r_i}\bullet\vec{r_p}} \qquad\qquad Eq\ (2.8)$$

Thus, the ratio intensity for the field of magnetic is :

$$\vec{H}_i = \frac{\vec{k}_i \times \vec{E}_i}{Z_o} = \frac{1}{Z_o}(E_{i\phi}\hat{\theta} - E_{i\theta}\hat{\phi})e^{jk\hat{r_i}\bullet\vec{r_p}} \qquad\qquad Eq\ (2.9)$$

where $y_0$ is free space impedance, PO approximation for the flowing of the current upon on the faces is:

$$\vec{J}_s. = 2\hat{n} \times \vec{H}_i = \frac{2}{y_o}(E_{i\phi}\hat{\theta} - E_{i\theta}\hat{\phi})e^{jkh} \qquad\qquad Eq\ (2.10)$$

## 2.6 Problem Formulation

Although, a lot of research work has been done in order to acquire correct estimation of RCS for flying aircrafts, however, no work has yet been proposed to calculate reflection coefficients in case of Ground-to-Aircraft and Satellite-to-Aircraft communication links. Furthermore, no concrete relationship has been established so far between RCS and reflection coefficient of the target body. Since, RCS and reflection coefficients are highly dependent upon the incident angle of the EM wave transmitted from RADAR transmitter; therefore, there is a need of investigating RCS and reflection coefficients against various incident angles in both Ground-to-Aircraft and Satellite-to-Aircraft scenarios.

## 2.7 Research Methodology

In order to address the above-mentioned problem in our study, we aim to acquire RCS estimation first by using well-established software tool known as POFACETS®

[36]. This software has been developed by David C. Jenn [37]. POFACETS® operates on Physical Optics (PO) approximation for predicting the RCSs of a complex targets. It utilizes the computational scientific distinctive of MATLAB® and its graphical-user-interface (GUI) functions to provide efficient calculation of RCS. In POFACETS®, the object needs to be in Stereo Lithography(.stl) format. Since, no (.stl) object file of a complete aircraft is available in the literature, therefore, we need to develop our own (.stl) object file of aircraft. For this purpose, we selected Aircraft A380 as our target. This is the world's largest commercial aircraft with the capacity to carry 544 passengers. By using official dimensions, we designed the realistic model of the Aircraft A380 in AutoCAD® as (.DWG) file and converted it to Stereo Lithography (.stl) format. The designed (.stl) file of the aircraft A380 was then used to simulate its RCS at different incident angles. To find accurate incident angles, we designed a geometrical models for the two proposed scenarios, i.e. Ground-to-Aircraft and Satellite-to-Aircraft communication links. The obtained RCSs of A380 at different incident angles were then used to find reflection coefficients of the target aircraft.

# Chapter 3

## SYSTEM MODEL

This chapter gives a brief overview of AutoCAD based Object Design in its section 3.1. In section 3.2, the description of the RCS Acquisition System is presented. In the end, section 3.3 and 3.4 present the two proposed scenarios for Ground-to-Aircraft and Satellite-to-Aircraft Communication Links.

## 3.1 AutoCAD based Object Design

AutoCAD® is a computer-aided design (CAD) software used for 3-D design, 2-D design and drafting. AutoCAD® is developed and marketed by Autodesk Incorporation. AutoCAD® Used as an architectural planning tool, engineering drafting tool, graphics design tool, and also used as an 3D printing tool. To make it easy for the engineering students, AutoCAD® made different versions such as AutoCAD Electrical, AutoCAD Mecinical and AutoCAD® civil. DWG (drawing) is the native file format for AutoCAD® and a basic standard for CAD data interoperability. For the design purposes we choose 19.1 version of the AutoCAD released in 2014.

### 3.1.1 To Specify the Drawing Units in AutoCAD

For every design configuration of the units are very important. Various imperial and metric units are available in AutoCAD®, and it allows us to change units according to our need. For our drawing setup we determine METER is the unit of measurements, while the rest of units specification is shown in Fig. 3.1.
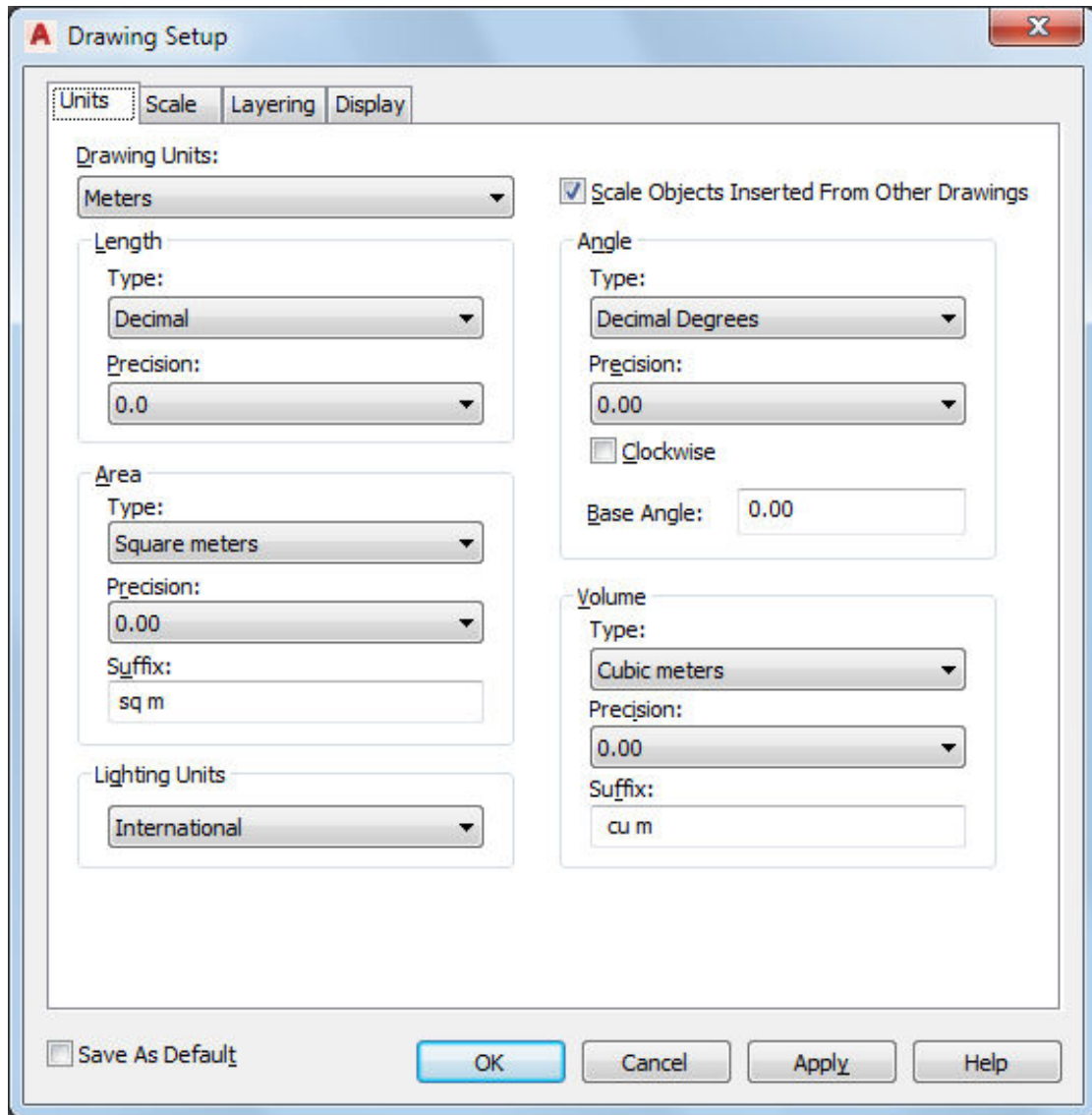
FIGURE 3.1: *Units Specification*

### 3.1.2 Size parameters of the Aircraft A380

In order to design a realistic model of the Aircraft, official dimension parameters would be required. Major dimensions are shown in Fig. 3.3, while the rest of the size parameters are given in table 3.1. On the basis of these official dimensions data we first design 2-D and later the 3D model of the Aircraft A380.

TABLE 3.1: Basic size parameters of the Aircraft A380

| Parameters | Values |
|---|---|
| Overall length | 73.72 m |
| Cabin length | 49.50 m |
| Fuselage width | 7.89 m |
| Max cabin width | 6.7 m |
| Wing span | 79.77 m |
| Height | 24.66 m |
| Wheelbase | 32.88 m |
| Max fuel capacity | 320 000 litres |
| Max zero fuel weight | 369 tonnes |
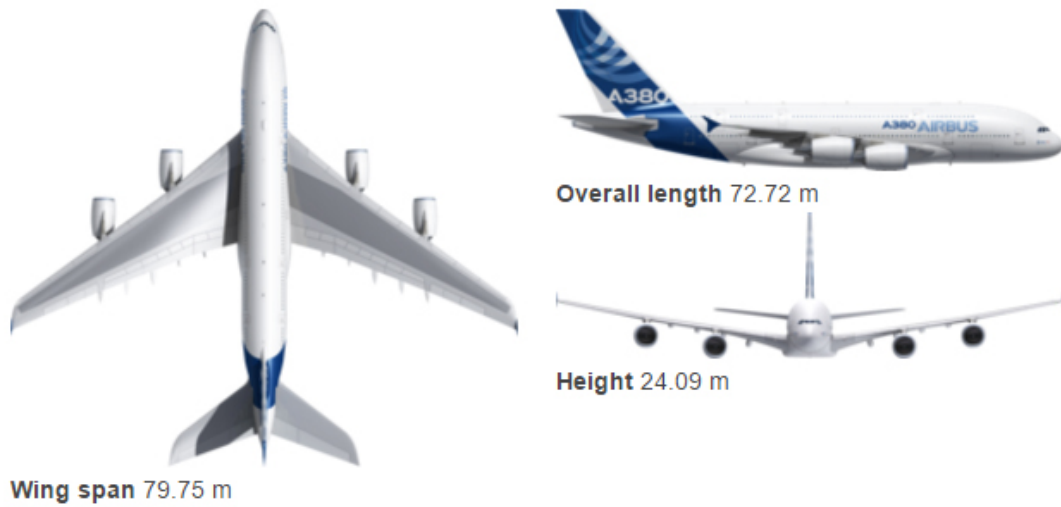


FIGURE 3.2: *Major Dimensions of the Aircarft A380*

### 3.1.3   2-D Modeling of Aircraft A380

In the latest versions of AutoCAD®, modeling environments are very easy and friendly as compared to the older versions. In this study, we use both environments, i.e '3D Modeling' and 'Drafting and Annotation'. We designed the 2-D model of the Aircraft A380 in drafting and annotation mode. During the designing basic tools are used such as line, polyline, circle, polygon, rectangle, trim, stretch, union and intersection. After making the 2-D model successful, we measured the dimensions and marked it as depicted in Fig. 3.3.
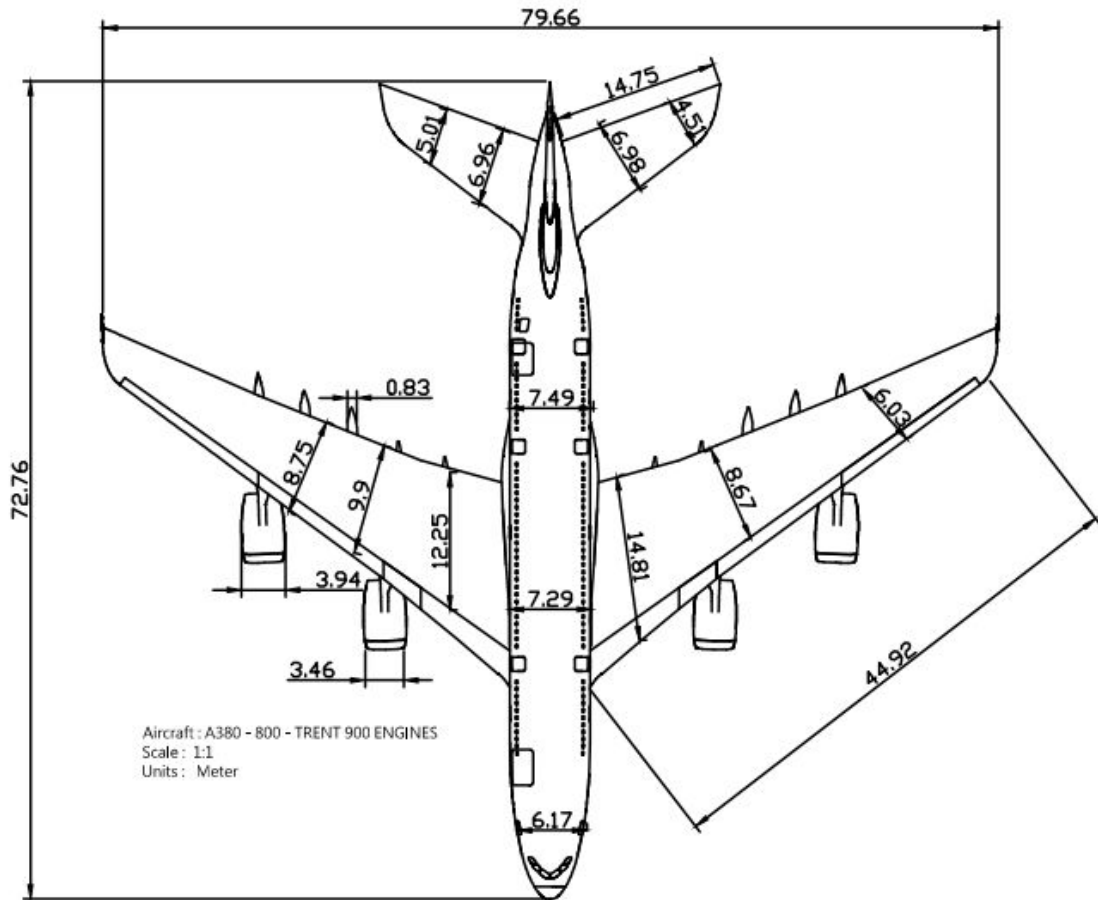
FIGURE 3.3: *2-D Model of Aircraft A380*

### 3.1.4  3-D Model of Aircraft A380

We first set the AutoCAD® modeling environment into 3D modeling environment. For coordinates configuration we select the default UCS system, which is aligned to the world coordinate system. Re-positioning and/or reorienting the User Coordinate System can be useful in the creation of 3D modeling. AutoCAD® has an ability to display realistic or conceptual visual styles of the designed models. Realistic modeling help us, that how our design models will look like in real life. Most of our design is done by using Mesh tools. Major tools used in the creation of 3-D modeling, *i.e* Cylinder (CYL), Pyramid (PYR), Union, subtract, smooth object, mesh-pyaramid, mesh-cylinder, extrude, defining layers, culling, and extrude

faces.
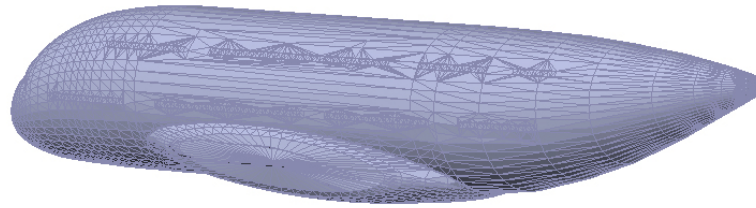


FIGURE 3.4: *Large cylindrical body of the Aircraft A380 with out wings*
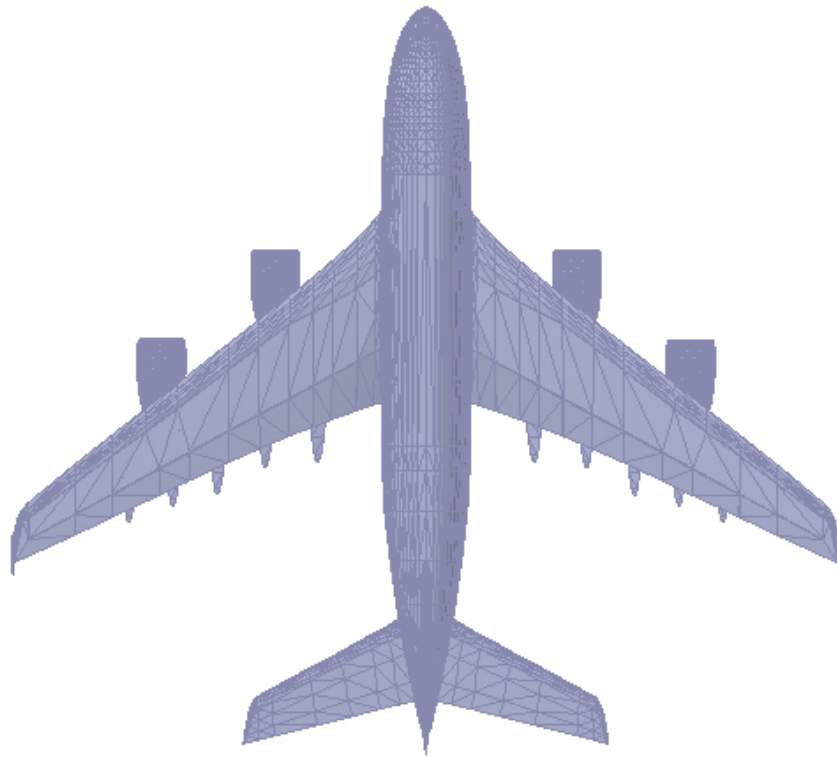


*(a) Top view*
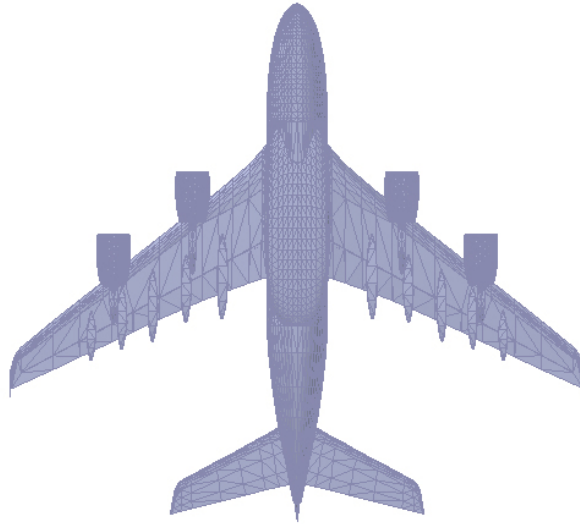
(b) Bottom view
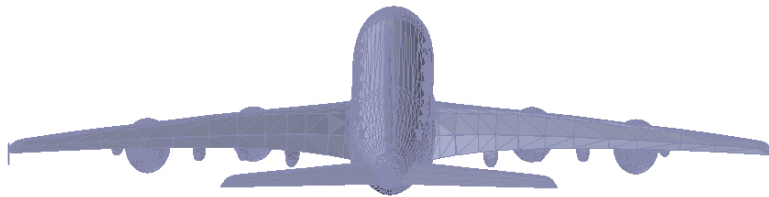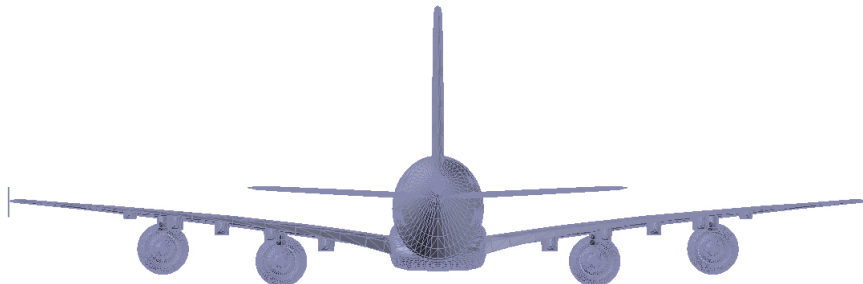


(c) Back view
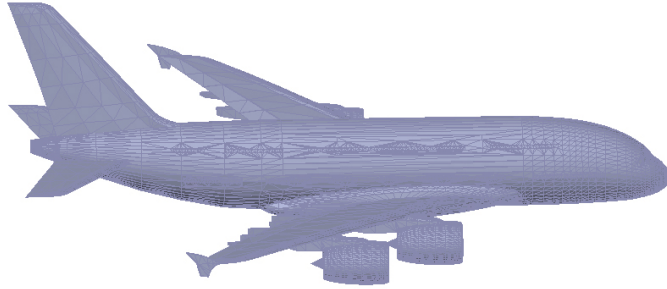


(d) Front view

FIGURE 3.5: *Various view prospectives of the A380 (a) Top view (b) Bottom view (c) Back view (d) Front view (e) Side view*

### 3.1.5   DWG to STL conversion

Stereolithography (SL) or Standard Triangle Language (STL) is one of several methods used to create 3D-printed objects. STL file format is supported by many other software packages; it is widely used for rapid prototyping, 3D printing and computer-aided manufacturing. STL files describe only the surface geometry of a three-dimensional object without any representation of color, texture or other common CAD model attributes. STL record portrays a crude unstructured triangulated surface by the unit typical and vertices of the triangles utilizing a three-dimensional Cartesian arrange framework.

Due to the use of triangles and large body size of the aircraft, it was hard to make an STL file in AutoCAD. In this study, AnyCAD exchanger 3D software tool, version 5.0 released in 2013 has been used for the conversion purposes. The use of this software tool is very easy. First we import DWG file of the Aircraft A380 in to software tool. On the exchanger menu we set the conversion between DWG to STL. Final look of Aircraft A380 STL version is shown in Fig. 3.6.
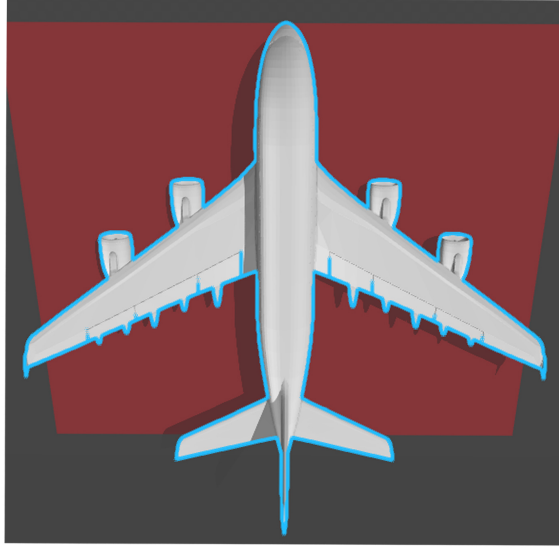
FIGURE 3.6: *STL version of Aircraft A380*

## 3.2 RCS Acquisition System

As discussed earlier, for RCS estimation, we use well-established software tool known as POFACETS®. This software has been developed by David C. Jenn [37]. POFACETS® operates on Physical Optics (PO) approximation for predicting the RCSs of complex objects. It uses the logical computational elements of MATLAB® and its graphical-UI (GUI) capacities to give efficient calculation of RCS. In this study, we use the latest and updated version (4.2 released in 2015) of POFACETS®. The latest version improved computational speed and accuracy.

### 3.2.1 POFACETS GUI and its capabilities

POFACETS® approximates scattering objects by arrays of triangles (facets) and uses superposition to compute the total RCS of the object [38]. Its GUI consists of five modules: **Design Model Manually, Design Model Graphically, Calculate Monostatic RCS, Calculate Bistatic RCS** and **Utilities** as shown in Fig. 3.7. POFACETS® operates in two graphical mode, i.e. **Design Model**
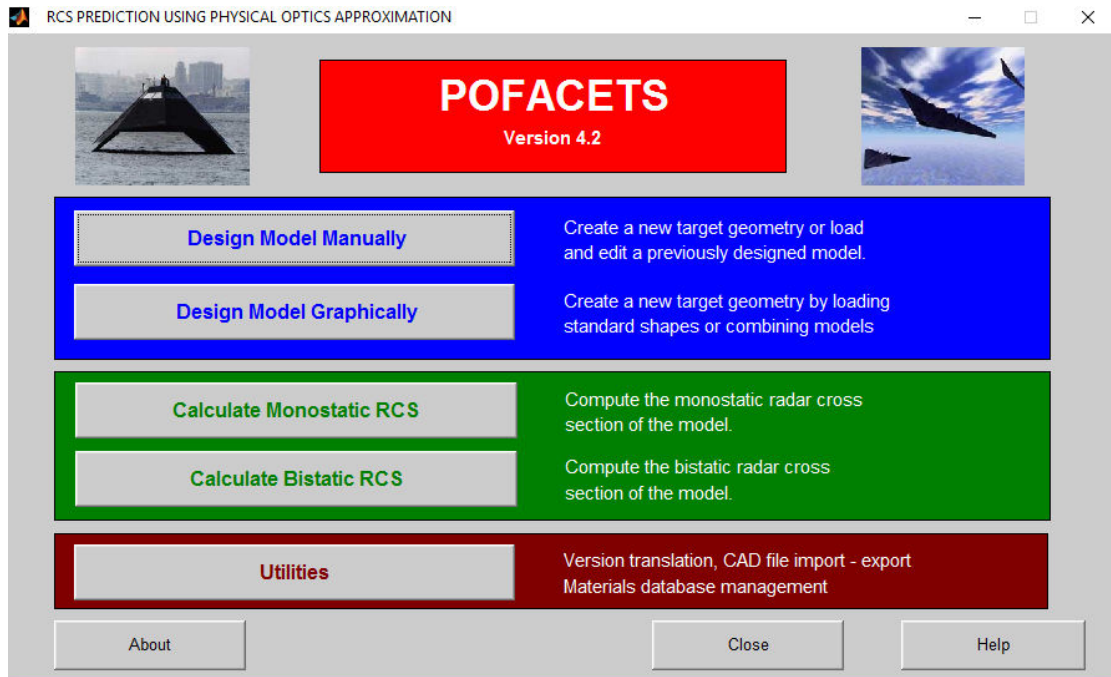
FIGURE 3.7: *Main GUI of POFACETS®*

**Manually** and **Design Model Graphically**. By clicking **Design Model Manually** tab, a new window will appear where user can create geometry of the target and can edit previously designed models. User can load and merge standard models easily with the help of **Design Mode Graphically** option. POFACETS® has a built-in library of common geometrical shapes, that are readily available for the users. 3D model of an object can be rotated, scaled, zoomed-in and zoomed-out in the designing mode. POFACETS® has an ability to calculate monostatic or bistatic RCS of the object for the parameters specified by the user and displays plots for its model geometry and RCS. **Calculate Bistatic RCS** tab GUI display is depicted in Fig. 3.8. To find RCS of an object, user will first upload the object file by clicking the **Load File** button. In incident angle dialog box, user can specify incident angles fields for $\theta$ and $\phi$. Observation or bistatic angle range can be set with feasible increment. By default, **Observation Angel** range is set from 0° to 360°. By selecting suitable values in **Surface Roughness**

fields, RCS of an object with a desired material can be simulated. With the help of built-in material library, users can set the surface resistivity for their objects. In **Surface Roughness**, users can specify roughness parameters i.e. corelation distance and standard diviation for an object. In **Computational Parameter** dialog box, user can specify incident polarization, operating frequency in GHz, and Taylor series. We can easily set mode of polarization for the incident angle, at incident polarization field Theta-TM polarization corresponds to vertical polarization, while Phi-TM polarization corresponds to horizontal polarization. For
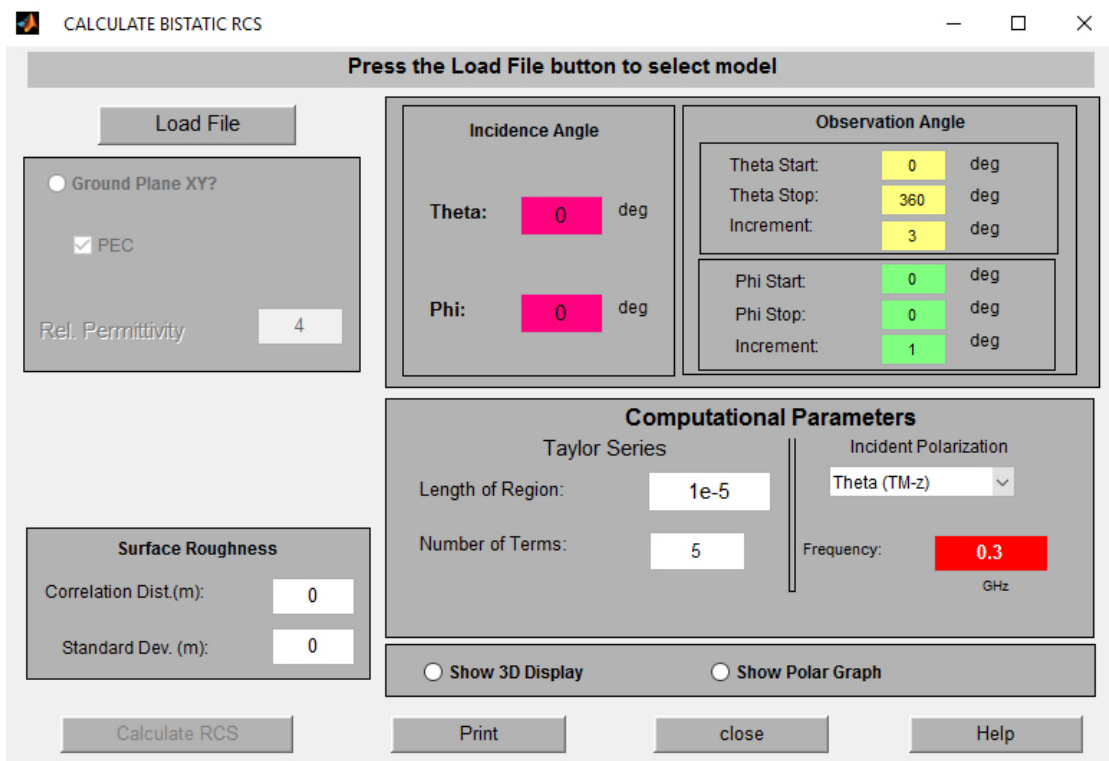


FIGURE 3.8: *Bistatic RCS GUI*

more accurate results, users can increase the number of terms in Taylor series field. As an increase in the number of terms reduces the computational speed; therefore, there is a trade-off between time and accuracy. Before going to click on **Calculate RCS** button, there are two buttons available for users in the **Computational Parameter** dialogue box, i.e. Show 3D Display and Show Polargraph

Graph. This will display the linear simulated RCS graph, if none of the button has been selected. Under **utilities** tab, more options including Import file, export file, and change in material database. Moreover, users can import AutoCAD®️ (.STL) file to POFACETS®️ with the help of **Utility** tab.

## 3.3    Satellite-to-Aircraft scenario

The word 'satellite' refers to a machine or natural body that is launched into space, to orbits a planet. In the solar system, Earth and moon are known to be natural satellites due to their continuous rotation around the sun and Earth. In space thousands of man-made or artificial satellites orbit Earth continuously. Different types of satellites have been made for different purposes. Satellites can be used for a wide array of applications such as environmental and climate monitoring, navigation and communication systems, television and telephone, safety and development, and for the earth observation and space science.

In this study we considered a geostationary satellite for the scenario of Satellite-to-Aircraft Communication Link. The reason for considering geostationary satellite is its high bandwidth and coverage over a large geographical area. Geostationary satellites are in a geostationary orbit around the earth, placed at an altitude of approximately 35,801 kilometers (22,200 miles) above sea level. It revolves in the same direction the Earth is turning (west to east) at speed of 1.91 miles per second. Three such satellites, each separated by 1220 degrees of longitude, can provide coverage of the entire planet. Each satellite has distinctive Equivalent Isotropically Radiated Power (EIRP). EIRP is the result of the power provided to the information terminal of the reception apparatus and the recieving wire transmit pick up. Regularly the EIRP is given in dBi, or decibels over isotropic. EIRP of Geostationary satellite is portrayed in Fig. 3.9.

  In this scenario, we assume that an aircraft A380 is flying at altitude of 10km above the ground. There is line of sight communication between geostationary
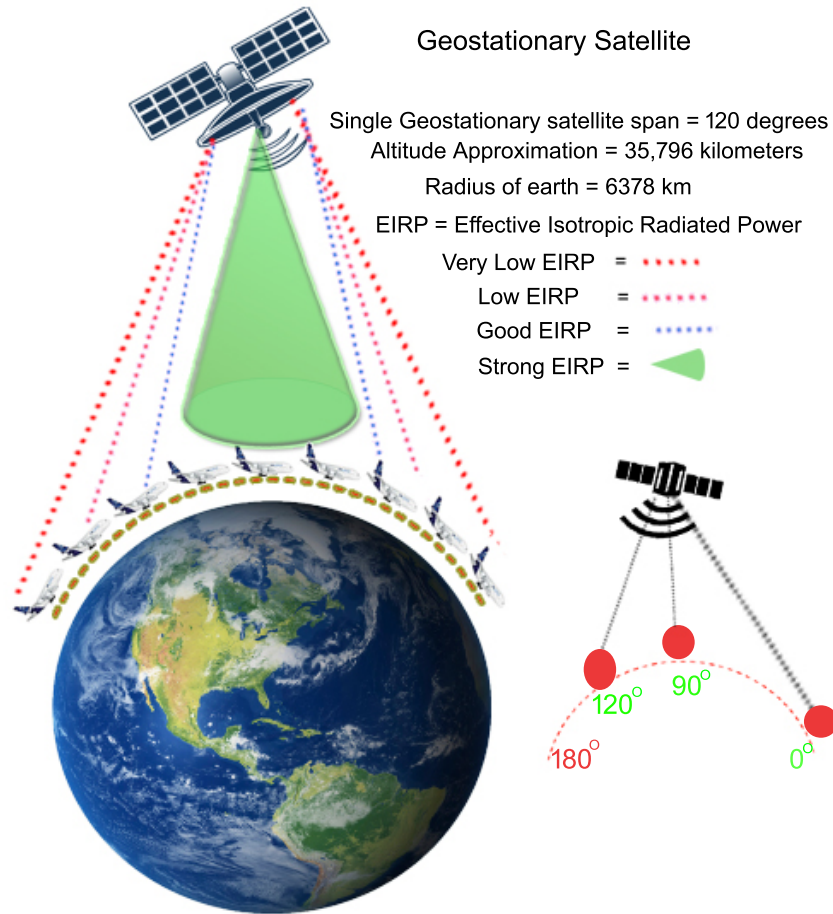
FIGURE 3.9: *Typical scenario of EIRP in the case of geostationary satellite*

satellite and Aircraft A380. During communication Aircraft can receive EM waves continuously. In order to find the accurate angles for the incident signals, we proposed a geometrical model for Satellite-to-Aircraft scenario. The geometrical model is depicted in Fig. 3.10.

The list of variables and some fixed values that have been used during calculation are listed below.

A = centre of the Earth

B = position of aircraft on the Earth's surface

G = satellite

b = distance from the centre of the earth to the satellite

a = distance from the aircraft to the satellite
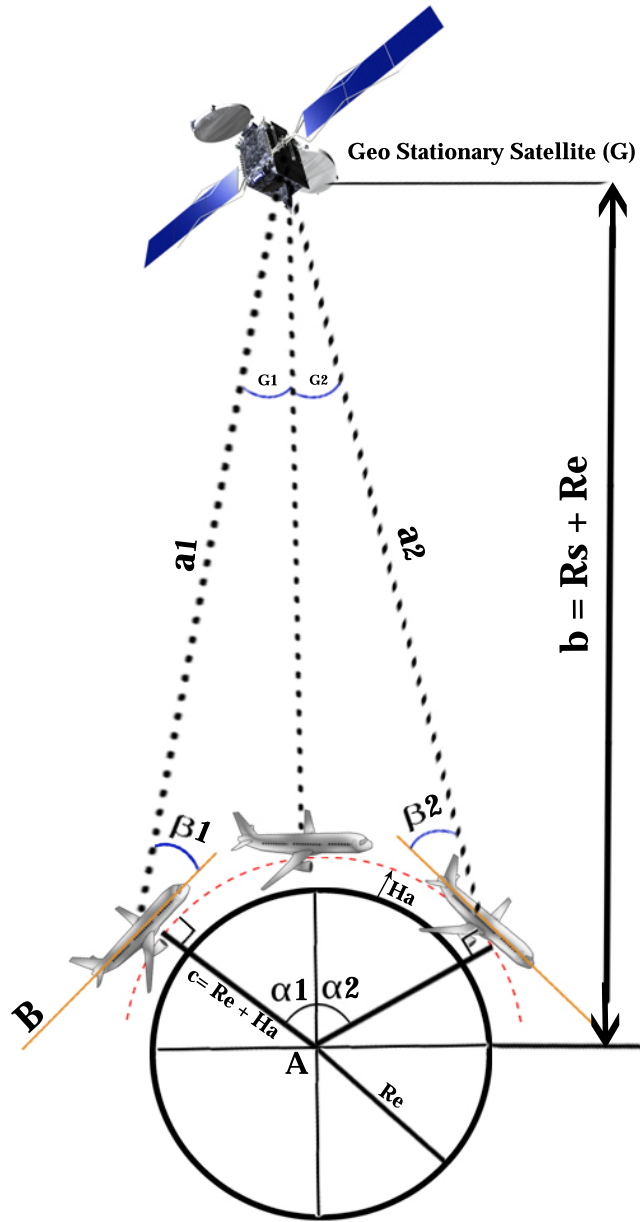
FIGURE 3.10: *Geometrical model of Satellite-to-Aircraft scenario*

Re = radius of earth (6378km)

Rs = altitude of satellite, measured from earth's surface (35796km)

Ha = altitude of the aircraft above the ground (10km)

G1 and G2 = angles on diagram; angles at satellite between center of Earth and observers on the ground.

B = 90 degrees (the angle between the radius from A and the horizon).

we assume that aircraft is an north and south equator. Therefore, we use longitude angles, i.e. $\alpha_1 = 60°$ and $\alpha_2 = -60°$ for the Aircraft A380. The included angles $(\alpha_1)$, $(\alpha_2)$ and lengths (b and c) are known. Therefore, we must start solving the triangle by using the cosine rule:

$$a_1^2 = b^2 + c^2 - 2bc \cos \alpha_1 \qquad\qquad Eq\ (3.1)$$

$$a_2^2 = b^2 + c^2 - 2bc \cos \alpha_2 \qquad\qquad Eq\ (3.2)$$

In order to find the distance from the aircraft to the satellite $(a_1)$, we put known lengths and angle into *Eq (1.1)*, we get:

$$
\begin{aligned}
a_1^2 &= (R_e + R_s)^2 + (R_e + H_a)^2 - (2 \times (R_s + R_e) \times (R_e + H_a) \times \cos 60°) \\
&= (42164000)^2 + (6388000)^2 - (2 \times (42164000) \times (6388000) \times 0.5)\mathrm{m}^2 \\
&= \sqrt{1.54926 \times 10^{15}} = 39360714.02\mathrm{m}
\end{aligned}
$$

In order to calculate $\beta 1$ angel, we will first calculate G1 by using sine rule.

$$a_1/\sin \alpha_1 = c/\sin G_1 \qquad\qquad Eq\ (3.3)$$

We can rewrite this equation in terms of $G_1$:

$$G_1 = \sin^{-1} \times (c \sin \alpha_1)/a_1 \qquad\qquad Eq\ (3.4)$$

by putting the known values of $\alpha_1$, $a_1$ and c in *Eq (3.4)*, we get:

$$G_1 = 8.0797°$$

To find the $\beta 1$ angel, we subtract $\alpha_1 + G_1$ from 90 degrees. Therefore, $\beta 1 = 90 - (\alpha_1 + G_1) = 90 - (60 + 8.079) = 21.921°$.

POFACETS® use clockwise rotation is a mode of reference. $\beta 1$ angle is not feasible for POFACETS®. In order to make it feasible, we subtract $\beta 1$ from 90 degrees (90 - $\beta 1$). Incident angle $\beta 1$ for POFACETS® is now equals to 68.079 degrees.
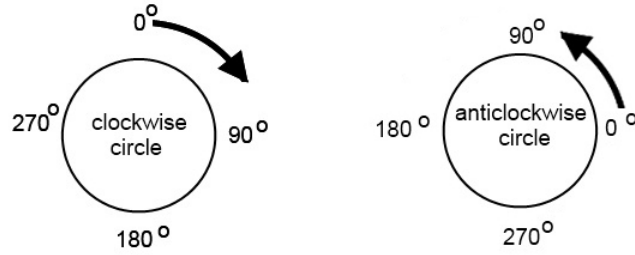


FIGURE 3.11: *Clockwise and anticlockwise mode of rotations*

Find $\beta 2$:

By putting known lengths and $\alpha_2$ angel in *Eq (3.2)*, we get:

$$
\begin{aligned}
a_2^2 &= (R_e + R_s)^2 + (R_e + H_a)^2 - (2 \times (R_s + R_e) \times (R_e + H_a) \times \cos(-60°) \\
&= (42164000)^2 + (6388000)^2 - (2 \times (42164000) \times (6388000) \times 0.5)\text{m}^2 \\
&= \sqrt{1.54926 \times 10^{15}} = 39360714.02\text{m}
\end{aligned}
$$

by using *Eq (3.4)*, we can find angle ($G_2$) for satellite.

G2 = -8.0797°.

To find the $\beta 2$ angel, we subtract $\alpha_2$ + $G_2$ angles from 90 degrees.

Therefore, $\beta 2$ = 90 - ($\alpha_2$ + $G_2$) = 90 - (-60 + (-8.079)) = 158.079°.

In order to make $\beta 2$ feasible for POFACETS®, we subtract 90 degrees from $\beta 2$ ( 90 - $\beta 2$ ). Incident angle $\beta 2$ for POFACETS® is now equals to -68.079 degrees.

TABLE 3.2: Setting Incident Angles to be used in POFACETS®

| Incident angle | Angle taken anticlockwise with respect to horizontal | Correspondly angle to be used in POFACETS® |
|---|---|---|
| $\beta 1$ | 21.921° | 68.079° |
| Perpendicular | 90° | 0° |
| $\beta 2$ | 158.079 | - 68.079° |
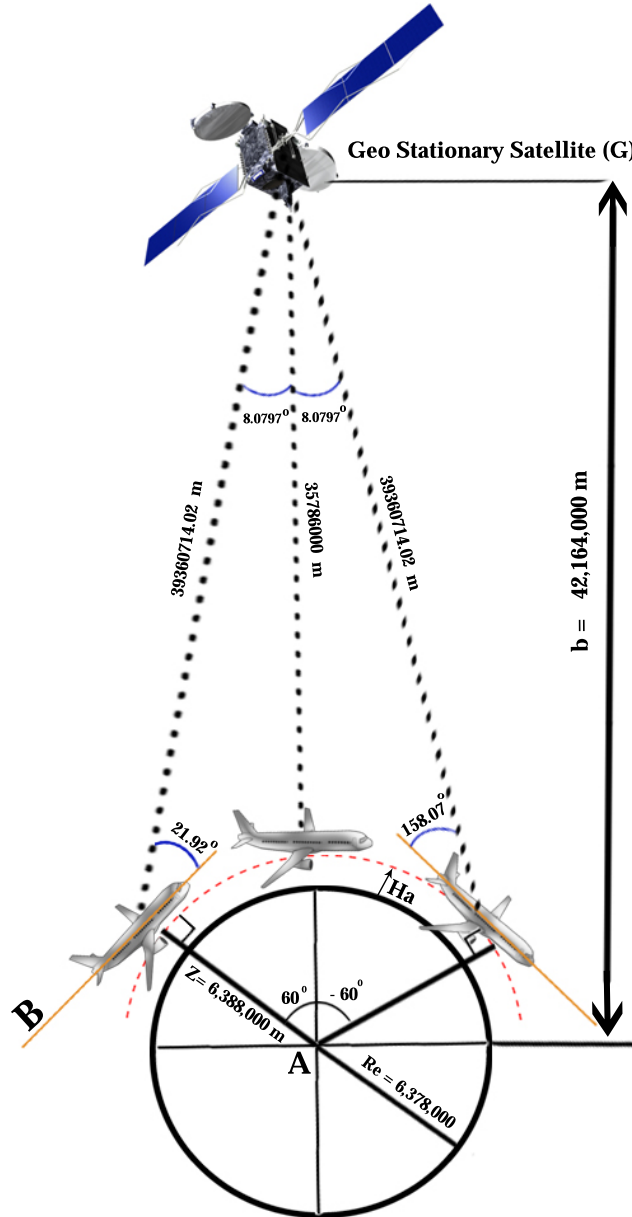


FIGURE 3.12: *Geometircal model of Satellite-to-Aircraft scenario after calculation*

44

## 3.4 Ground-to-Aircraft scenario

In this scenario we assume that Aircraft A380 is flying from the ground with an altitude of 10.688 km. The maximum official altitude range for the passenger Aircraft is 10.68km. For the communication purposes there is fixed radar station available on the ground. We assume that there is no hurdles or obstacles present in free space, and there is a Line of Sight (Los) communication between the Aircraft A380 and ground radar station. Every radar station has their own coverage capability. Mostly the radius of air cell depends on the maximum span of the generated signal beam.

Maximum possible radius of air cell [39].

$$r_{\text{cmax}} = \cos^{-1}\left(\frac{r_{\text{e}}}{r_{\text{e}} + h_{\text{a}}}\right)\frac{\pi r_{\text{e}}}{180°} \qquad\qquad Eq\ (3.5)$$

By setting $r_{\text{e}} = 6378.137$ km (Radius of Earth) and $h_{\text{a}} = 10.688$ km (Altitude of Aircraft). After putting these values in *Eq (3.5)*, we get: $r_{\text{cmax}} = 368.98$ km. With the help of tangent rule we can easily calculate the angle of the incident signal. The geometrical model of Ground-to-Aircraft scenario has been depicted in Fig. 3.13.

$$\tan\left(\frac{\theta}{2}\right) = \frac{r_{\text{cmax}}}{h_{\text{a}}} \qquad\qquad Eq\ (3.6)$$

After applying the tangent rule and by putting the known values of $r_{\text{cmax}}$ and $h_{\text{a}}$ in *Eq (3.6)*, we get:

$$\theta = 176.8951°$$

we can get maximum span of 88.4476° at each side by dividing $\theta$ by 2. To create a Los communication between the Aircraft and the Ground Station, the minimum angle should be require at which target is clearly visible to the Ground Station. We can easily find the minimum angle by subtracting 88.4476° from 90°. The minimum
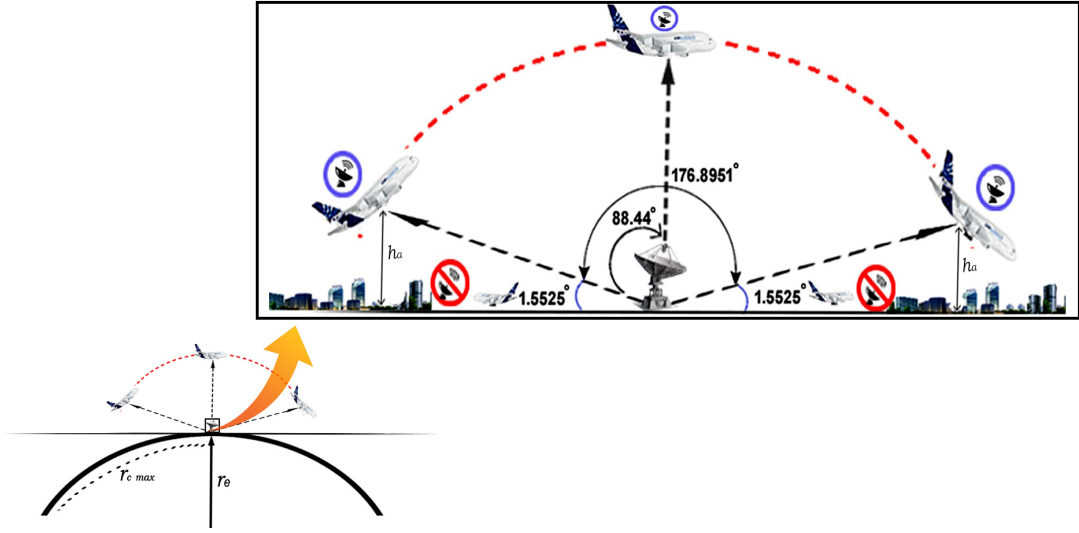
FIGURE 3.13: *Geometrical model of Ground-to-Aircraft scenario*

threshold angle for the Ground Station, to make a consistent Los communication with the target is now $\geq 1.5525°$. If the target is flying below the threshold angle or nearly to the earth surface then its hard for the Ground Station to stable its Los communication link with the target. The reason for the destabilization of Los communication link is high buildings, trees, towers and other obstacles. The graphical model of this senario has been depicted in Fig. 3.13. Encircled blue sign represents that target has a Los communication with the Ground Station, while the red encircled sign represents that target is not visible to the Ground Station. Our final results for this scenario would be based on these three angles $1.5525°$, $90°$ and $176.8951°$. The rest of the Geometrical model is very clear and easy to understand.

TABLE 3.3: Setting Incident Angles to be used in POFACETS®

| Incident angle for | Angle taken anticlockwise with respect to horizontal | Correspondly angle to be used in POFACETS® |
| --- | --- | --- |
| Right Aircraft | 1.55° | 88.4° |
| Middle Aircraft | 270° | 180° |
| Left Aircraft | 178.45° | -88.4° |

# Chapter 4

## RESULTS AND THEIR DESCRIPTION

This chapter presents the simulation results of RCS for the two scenarios as discussed in chapter 3. The results are evaluated over different incidence angles that influence the reflection properties of the target object.

## 4.1 Satellite-to-Aircraft Communication Link

In this study, we considered a geostationary satellite for the scenario of Satellite-to-Aircraft Communication Link. The reason for considering geostationary satellite is its utilization in airborne internet provision in aircrafts. Geostationary satellites are known for their high bandwidth and coverage over a large geographical area. Geostationary satellites are in a geostationary orbit around the earth, placed at an altitude of approximately 35,0 kilometers (22,00 miles) above sea level. It revolves in the same direction the Earth is turning (west to east) at speed of 1.91 miles per second. Three such satellites, each separated by 120 degrees of longitude, can provide coverage of the entire planet. In this scenario, we assume that an aircraft A380 is flying at altitude of 10km above the ground and there is line of sight communication between geostationary satellite and Aircraft A380.

### 4.1.1 Bistatic RCS and Reflection Coefficient on Incidence angle $\theta_i = 0°$

Fig. 4.1 shows the A380 aircraft model, imported from an STL file. With the help of 3D model, we can analyze the direction of the reflected signals easily. Yellow arrow represents the direction of the incidence signal while the red arrows represent the reflected or scattered signals from the Aircraft surface.

FIGURE 4.1: *3D representation of RCS calculation at incidence angle $\theta_i = 0°$*
*for the case of Aircraft-to-Satellite communication link*

Fig. 4.2 shows the behavior of bistatic RCS for the case of Aircraft-to-Satellite Communication Link. In this figure, RCS(dBsm) is plotted against Bistatic angle, $\theta$(deg), with POFACETS® an incidence angle of 0 degrees in $\phi = 0°$ plane. Observation direction or bistatic angle is varied from -90 to 90 degrees in the $\phi = 0°$ plane, using a signaling frequency of 2 GHz and the number of Taylor Series based polynomial terms set at 3. incidence wave polarization mode is set at linear-vertical polarization. Surface Roughness Correlation Distance and Standard Deviation terms are set to zero. At the POFACETS® incidence angle set at 0°, both Aircraft and geostationary satellite are perpendicular to each other. The maximum lobe at -3.75 degrees is the specular reflection from the top surface of
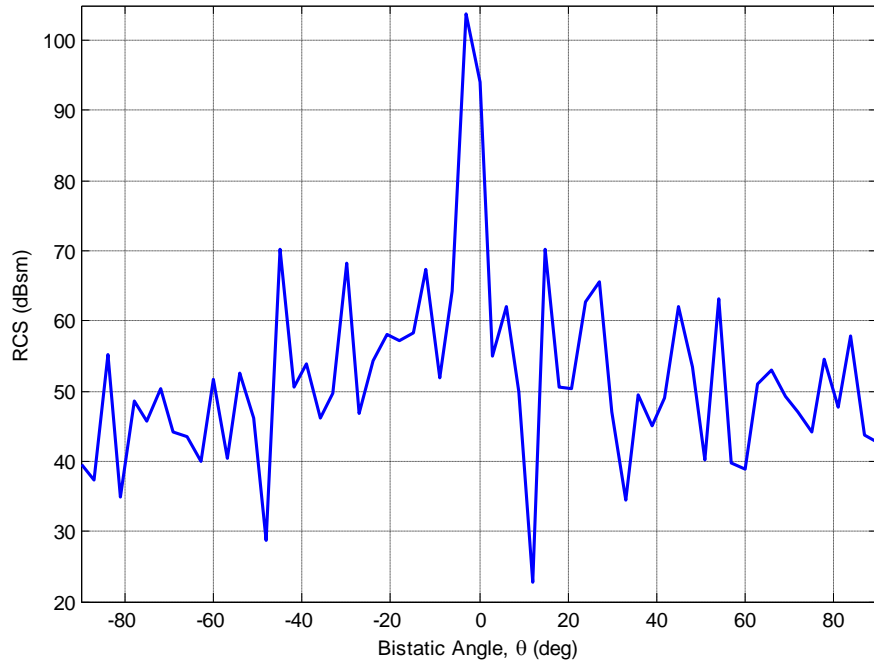
FIGURE 4.2: *RCS observation at incidence angle $\theta_i = 0°$ for the case of Aircraft-to-Satellite communication link*

the Aircraft. Other than the maximum lobe, there are multiple side lobes available as depicted in Fig. 4.2. Side lobes occur due to the large and complex body of the Aircraft. Complex body of the Aircraft will make the reflected signals to be scattered at directions other than the desired one. It can be observed that a geostationary satellite will now receive a strong reflected copy of the transmitted signal at -3.75 degrees. Although the apperance of the RCS spikes in graph, these have notably lower values (more than 70 dB below the largest value), as shown in the Fig. 4.2. It can be also noticed that the fluctuation in RCS behavior is mainly dependent on the shape of the target and incidence angle. Polar plot in Fig. 4.3 provide a more sophisticated way to present results for the anti clockwise angles in the full range of 0 to 360 degree. Here, for $\theta = -3.75°$ (or $\theta = 356.25°$ in polar) is the highest value and represents the major lobe of the polar plot. The resulting values of the RCS can be read in dBsm on the concentric circles in the
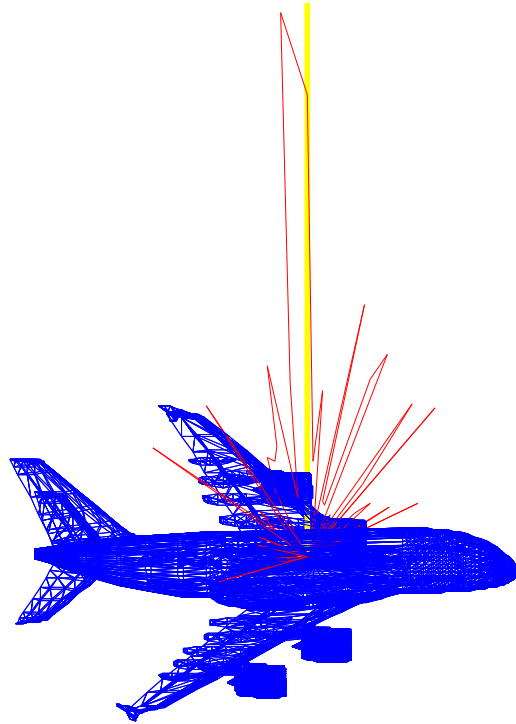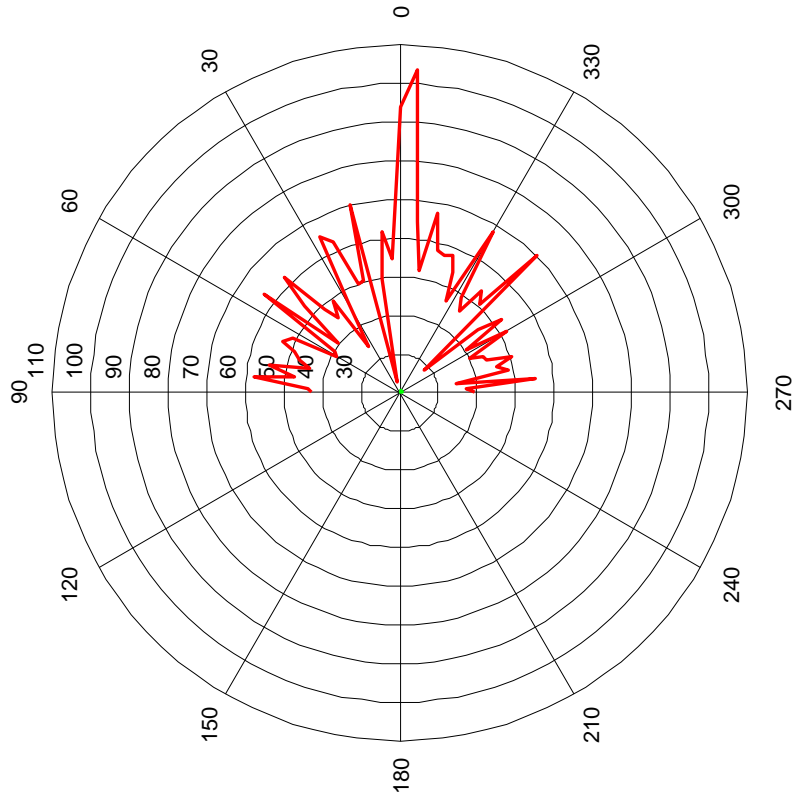
FIGURE 4.3: *Polar plot of RCS calculation at incidence angle $\theta_i = 0°$ for the case of Aircraft-to-Satellite communication link*

graph. RCS values from the plot in Fig. 4.2 when placed in *Eq (1.22)* on page 17, reflection coefficients at different observation angles are obtained. These reflection coefficients are listed in Table 4.1. It can also be observed that the reflection coefficient at $0°$ and $-3.75°$ are the highest.

TABLE 4.1: Characterization of reflection coefficient at incidence angle $\theta_i = 0°$
for the case of Satellite-to-Aircraft Communication Link

| Incidence angle | $d_1$(km) | Bistatic angles ($\theta$) | $d_2$(km) | $\sigma$ | $|\Gamma|$ |
|---|---|---|---|---|---|
| 0° | 35,790 | 50° | 55679 | 40 dBsm | $1.294 \times 10^{-6}$ |
| | | 40° | 46720 | 47 dBsm | $3.108 \times 10^{-6}$ |
| | | 30° | 41326 | 35 dBsm | $8.2691 \times 10^{-7}$ |
| | | 20° | 38086 | 50 dBsm | $4.835 \times 10^{-6}$ |
| | | 10° | 36342 | 23 dBsm | $2.207 \times 10^{-7}$ |
| | | 0° | 35790 | 95 dBsm | $8.862 \times 10^{-4}$ |
| | | -3.75° | 35866 | 109 dBsm | $4.439 \times 10^{-3}$ |
| | | -20° | 38086 | 58 dBsm | $12.147 \times 10^{-6}$ |
| | | -30° | 41326 | 68 dBsm | $36.951 \times 10^{-6}$ |
| | | -50 ° | 55679 | 29 dBsm | $3.621 \times 10^{-7}$ |

## 4.1.2 Bistatic RCS and Reflection Coefficient on Incidence angle $\theta_i = 68.079°$

In this section the incidence angle is now changed from $\theta_i = 0°$ to one extreme, i.e. $\theta_i = 68.079°$ in the $\phi = 0°$ plane, as discussed in section 3.7. The Observation direction or bistatic angle is varied from -90 to 90 degrees in the $\phi = 0°$ plane, using a frequency of 2 GHz and the number of Taylor Series terms set at 3. The 3D model of the Aircraft for the incidence angle $\theta_i = 68.079°$ is depicted in Fig. 4.4. The position of the geostationary satellite and Aircraft is no more perpendicular to each other.

FIGURE 4.4: *3D representation of RCS calculation at incidence angle* $\theta_i = 68.079°$ *for the case of Aircraft-to-Satellite communication link*

incidence EM waves will now impinge at the front cylindrical body, engines and wings. Due to change in incidence angle according to our scenario, it can be observed that the behavior of the RCS is now totally changed as compared to the previous result. It can be noticed that the energy of the reflected signals from the Aircraft body is now dispersed. The maximum lobe at $\theta = -50°$ (or $310°$ in polar) is the specular reflection from the body of the Aircraft. Albeit different RCS spikes show up in the chart, these have significantly bring down qualities (more than 50 dB underneath the most elevated esteem), as demonstrated in the Fig. 4.5.
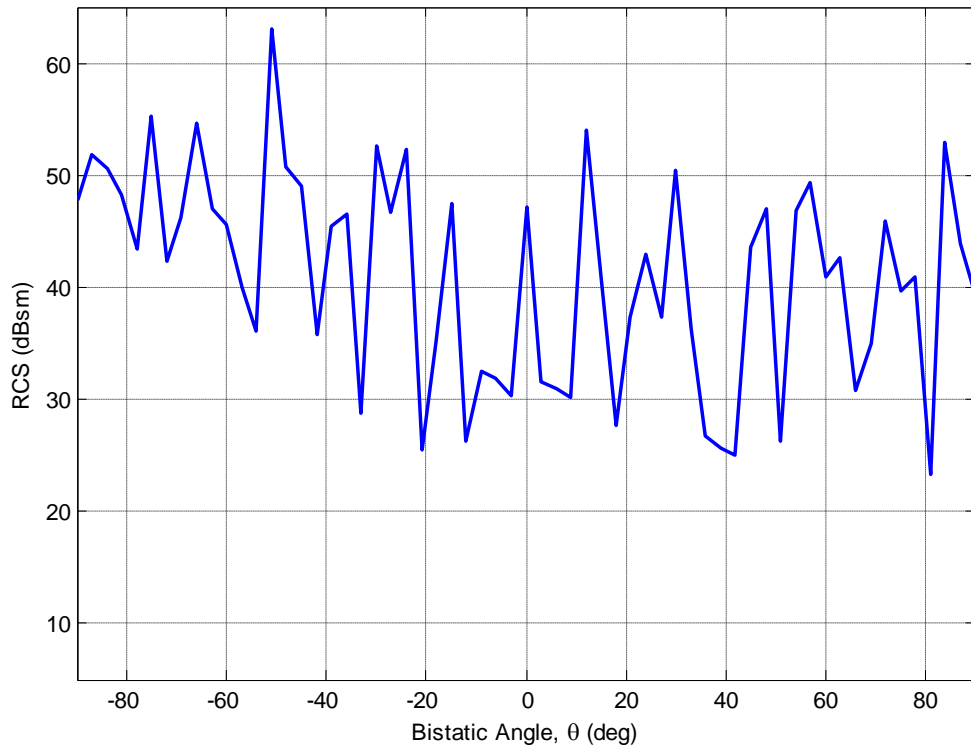
FIGURE 4.5: *RCS observation at incidence angle $\theta_i = 68.079°$ for the case of Aircraft-to-Satellite communication link*

The rapid change in the behavior of the RCS can also be seen in polar plot, shown in Fig. 4.6. However, it can also be observed that the gain or ratio of major spike to minor spikes is reduced at incidence angle of 68.079° as compared to that at incidence angle of 0°.
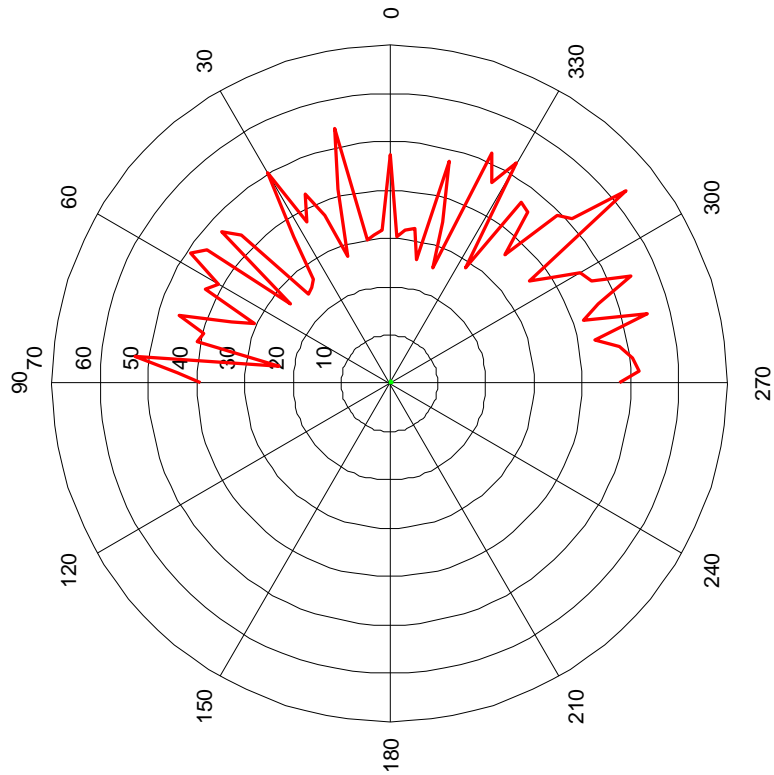
FIGURE 4.6: *Polar plot representation of RCS calculation at incidence angle* $\theta_i = 68.079°$ *for the case of Aircraft-to-Satellite communication link*

RCS values from the plot in Fig. 4.5 when placed in *Eq (1.22)* on page 17, reflection coefficients at different observation angles are obtained. These reflection coefficients are listed in Table 4.2. It can also be observed that the reflection coefficient at $-50°$ is higher as compared to the others having extreme low Gains.

TABLE 4.2: Characterization of reflection coefficient at incidence angle $\theta_i = 68.079°$ for the case of Satellite-to-Aircraft Communication Link

| Incidence angle | $d_1$(km) | Bistatic angles ($\theta$) | $d_2$(km) | $\sigma$ | $|\Gamma|$ |
|---|---|---|---|---|---|
| 68.079° | 95867 | 50° | 55679 | 26 dBsm | $1.598 \times 10^{-7}$ |
| | | 40° | 46721 | 25 dBsm | $1.597 \times 10^{-7}$ |
| | | 30° | 41327 | 50 dBsm | $3.089 \times 10^{-6}$ |
| | | 20° | 38087 | 38 dBsm | $8.222 \times 10^{-7}$ |
| | | 15° | 37053 | 55 dBsm | $5.937 \times 10^{-6}$ |
| | | 10° | 36342 | 30 dBsm | $3.3860 \times 10^{-7}$ |
| | | 0 ° | 35790 | 47 dBsm | $2.423 \times 10^{-6}$ |
| | | -10° | 36342 | 30 dBsm | $3.386 \times 10^{-7}$ |
| | | -20° | 38087 | 27 dBsm | $2.317 \times 10^{-7}$ |
| | | -30° | 41327 | 53 dBsm | $4.364 \times 10^{-6}$ |
| | | -40° | 46721 | 42 dBsm | $1.130 \times 10^{-6}$ |
| | | -50 ° | 55679 | 65 dBsm | $1.424 \times 10^{-5}$ |

## 4.1.3 Bistatic RCS and Reflection Coefficient on Incidence angle $\theta_i = -68.079°$

In this section the incidence angle is changed from $\theta_i = 68.079°$ to one extreme, i.e. $\theta_i = -68.079°$ in the $\phi = 0°$ plane, as discussed in section 3.7. The Observation direction or bistatic angle is varied from -90 to 90 degrees in the $\phi = 0°$ plane, using a signaling frequency of 2 GHz and the number of Taylor Series based polynomial terms set at 3. The 3D model of the Aircraft is depicted in Fig. 4.7. With the help of 3D model, we can clearly observe that which body parts of the Aircraft create high or low spike of RCS. The Orientation of the geostationary satellite and Aircraft is changed according to the scenario discussed in section 3.7. The major lobe at 39 degrees is the specular reflection occur from the fuselage of the Aircraft. Albeit different RCS spikes show up in the chart, these have significantly
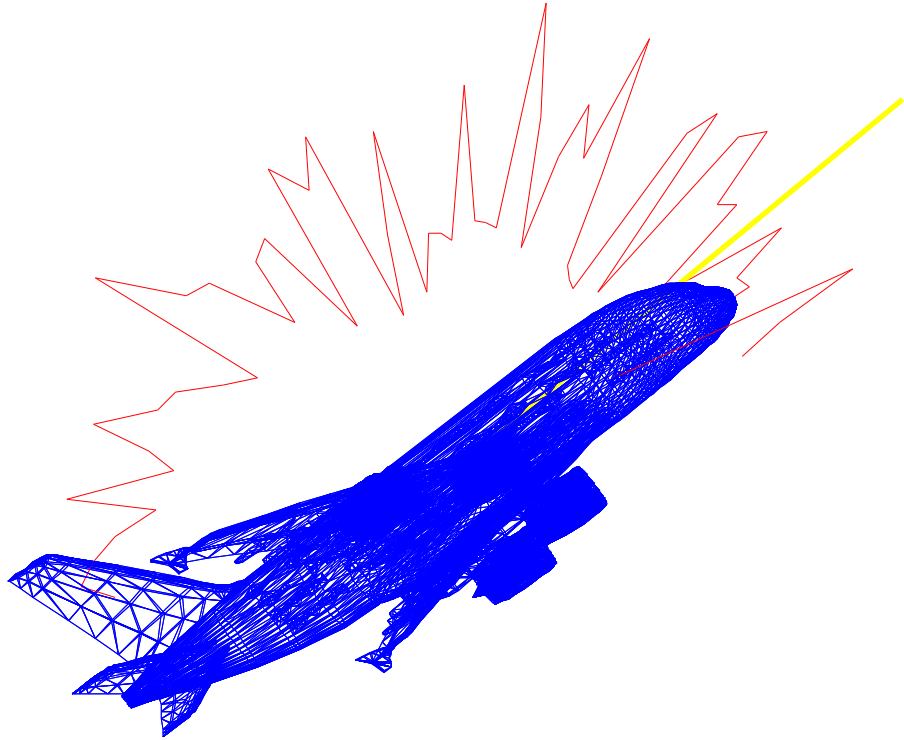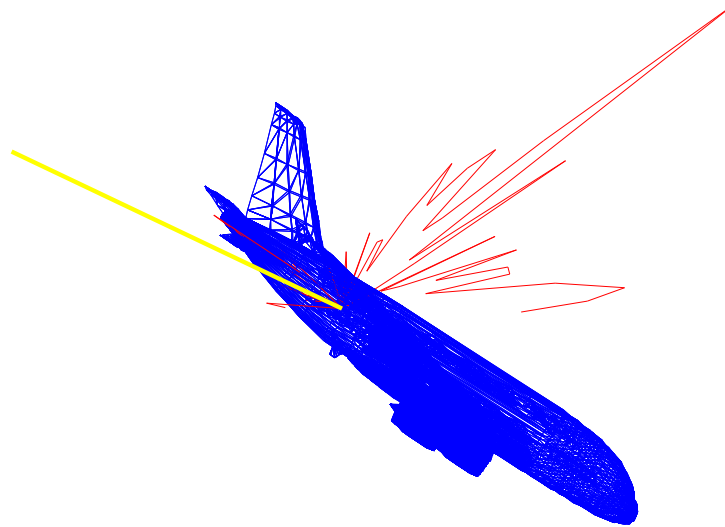
FIGURE 4.7: *3D representation of RCS calculation at incidence angle* $\theta_i = -68.079°$ *for the case of Aircraft-to-Satellite communication link*

bring down qualities (more than 50 dB underneath the most elevated esteem), as demonstrated in the Fig. 4.8. Due to change in incidence angle according to our scenario, it can be observed that the behavior of the RCS is now totally changed as compared to the previous result. However, it can also be observed that the gain or ratio of major spike to minor spikes is increased at incidence angle of $-68.079°$ as compared to that at incidence angle of $68.079°$. Maximum lobes and changes in the behavoir of the RCS can be observed in polar plot, as shown in Fig. 4.9.
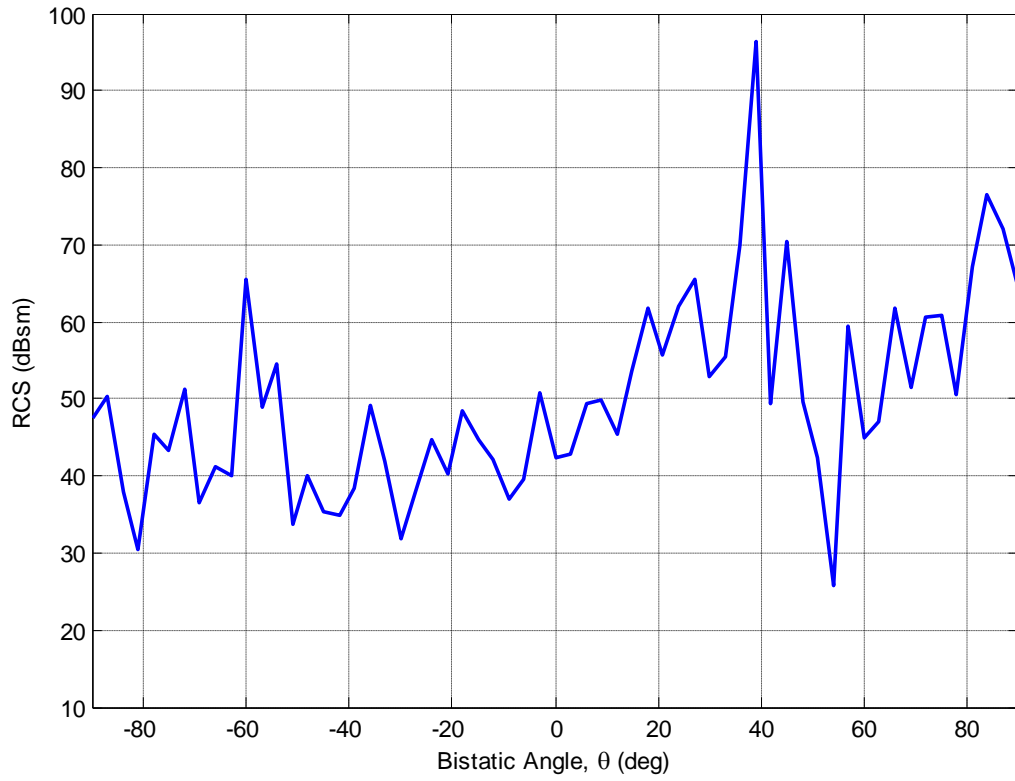
FIGURE 4.8: *RCS observation at incidence angle* $\theta_i = -68.079°$ *for the case of Aircraft-to-Satellite communication link*
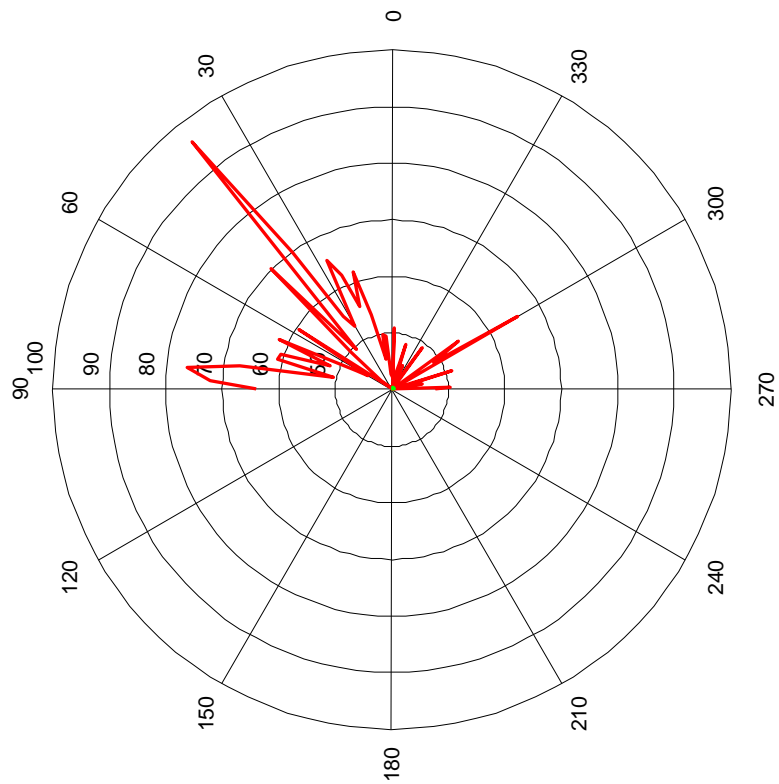
RCS values from the plot in Fig. 4.8 when placed in *Eq (1.22)* on page 17, reflection coefficients at different observation angles are obtained. These reflection coefficients are listed in Table 4.3. It can also be observed that the reflection coefficient at 39° is higher as compared to the others values of reflection coefficients.

TABLE 4.3: Characterization of reflection coefficient at incidence angle $\theta_i = -68.079°$ for the case of Satellite-to-Aircraft Communication Link

| Incidence angle | $d_1$(km) | Bistatic angles ($\theta$) | $d_2$(km) | $\sigma$ | $|\Gamma|$ |
|---|---|---|---|---|---|
| -68.079° | 95867 | 39° | 46053 | 98 dBsm | $7.204 \times 10^{-4}$ |
| | | 25° | 39490 | 65 dBsm | $1.7940 \times 10^{-5}$ |
| | | 20° | 38087 | 57 dBsm | $7.328 \times 10^{-6}$ |
| | | 15° | 37053 | 46 dBsm | $2.1067 \times 10^{-6}$ |
| | | 10° | 36342 | 50 dBsm | $3.3860 \times 10^{-6}$ |
| | | 0° | 35790 | 43 dBsm | $1.529 \times 10^{-6}$ |
| | | -10° | 36342 | 38 dBsm | $8.505 \times 10^{-7}$ |
| | | -15° | 37053 | 43 dBsm | $1.491 \times 10^{-6}$ |
| | | -20° | 38087 | 41 dBsm | $1.161 \times 10^{-6}$ |
| | | -25 ° | 39490 | 38 dBsm | $8.0136 \times 10^{-7}$ |
| | | -30 ° | 41327 | 32 dBsm | $3.889 \times 10^{-7}$ |
| | | -60 ° | 71580 | 65 dBsm | $1.224 \times 10^{-5}$ |

## 4.2 Ground-to-Aircraft Communication Link

In this scenario, we assume that Aircraft A380 is flying above the ground with an altitude of 10 km. The maximum official altitude range for the passenger Aircraft is around 10km. For the communication purposes, there is a radar station present on the ground. We assume that there is no hurdles or obstacles present in free space, and there is a Line of Sight (LoS) communication between the Aircraft A380 and ground radar station.

### 4.2.1 Bistatic RCS and Reflection Coefficient on Incidence angle $\theta_i = 180°$

Fig. 4.10 shows the 3D model of the Aircraft. With the help of 3D model, we can analyze the direction of the reflected or scattered signals easily. we can clearly observe that which part of the Aircraft body create high or low spikes of RCS. Fig. 4.11 shows the behavior of bistatic RCS for the case of Ground-to-Aircraft



FIGURE 4.10: *3D representation of RCS calculation at incidence angle $\theta_i = 180°$ for the case of Ground-to-Aircraft Communication Link*

communication link. In this figure, RCS(dBsm) is plotted against Bistatic angle, $\theta$(deg), with POFACETS® an incidence angle of 180 degrees in $\phi = 0°$ plane. Observation direction or bistatic angle is varied from 90 to 270 degrees according to the POFACETS® clock-wise mode of rotation in the $\phi = 0°$ plane, using a

signaling frequency of 2 GHz and the number of Taylor Series based polynomial terms set at 3.
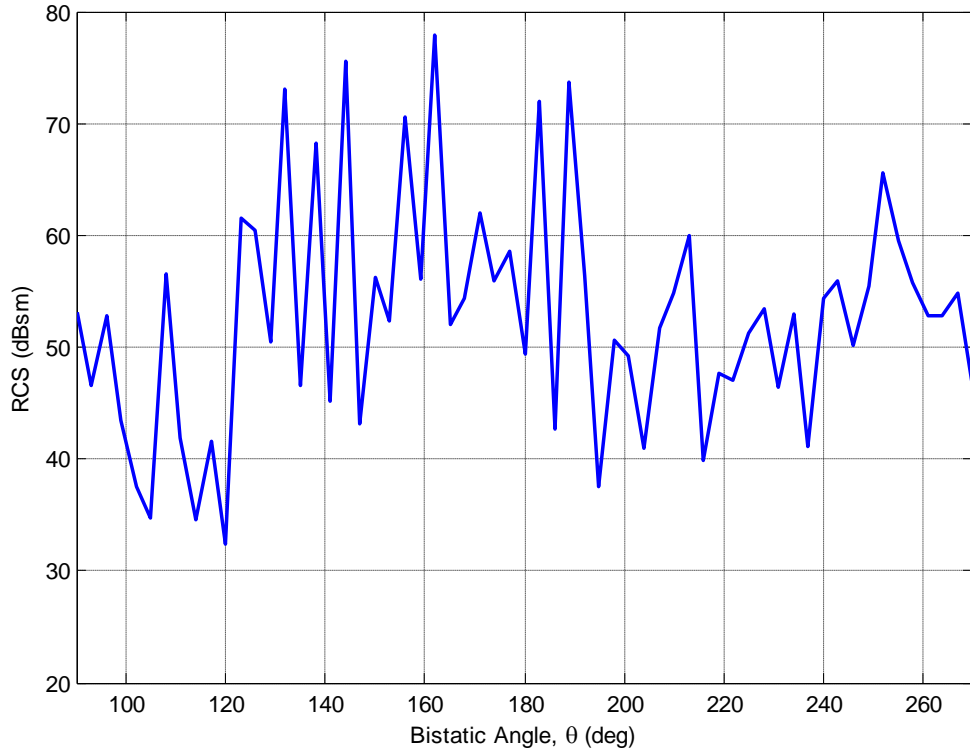


FIGURE 4.11: *RCS observation at incidence angle $\theta_i = 180°$ for the case of Ground-to-Aircraft Communication Link*

incidence wave polarization mode set at linear-vertical polarization. Surface Roughness Correlation Distance and Standard Deviation terms are set to zero. Locality of the ground radar station and Aircraft are depicted in Fig. 3.13. In this case ground radar station continuously radiate EM waves towards the lower surface of the Aircraft body. There is no clear indication available for maximum gain at some considerable angles, because the RCS spikes for maximum and side lobes are approximately equal. Albeit different RCS spikes show up in the chart, these have significantly bring down qualities (more than 50 dB underneath the most

elevated esteem), as demonstrated in the Fig. 4.11. Due to change in orientation and incidence angle respectively, It can be noticed that the energy of the reflected signals from the bottom surface of the Aircraft is now dispersed in free space over a different bistatic angles. The main cylindrical body of the Aircraft and its leading edges of the wings create multiple strong RCS spikes. Change in the behavior of the RCS can also be observed in polar plot, as shown in Fig. 4.12.



FIGURE 4.12: *Polar plot representation of RCS calculation at incidence angle* $\theta_i = 180°$ *for the case of Ground-to-Aircraft Communication Link*

RCS values from the plot in Fig. 4.11 when placed in *Eq (1.22)* on page 17, reflection coefficients at different observation angles are obtained. For the case of Ground-to-Aircraft Communication Link, distance $d_1$ is fixed at 10km. It can be noticed that the reflection coefficient is increased as the $d_1$ reduced to 10km as

compared to that at $d_1 = 35790$km for Satellite-to-Aircraft Communication Link. These reflection coefficients are listed in Table 4.4. It can also be observed that the reflection coefficient values are at $190°$ is higher as compared to the others values of reflection coefficients.

TABLE 4.4: Characterization of reflection coefficient at incidence angle $\theta_i = 180°$ for the case of Ground-to-Aircraft Communication Link

| Incidence angle | $d_1$(km) | Bistatic angles $(\theta)$ | $d_2$(m) | $\sigma$ | $|\Gamma|$ |
|---|---|---|---|---|---|
| 180° | 10 | 140 ° | 13054 | 46 dBsm | 0.009 |
| | | 150° | 11547 | 55 dBsm | 0.029 |
| | | 160° | 10642 | 58 dBsm | 0.043 |
| | | 170 ° | 10154 | 63 dBsm | 0.079 |
| | | 180 ° | 10000 | 50 dBsm | 0.017 |
| | | 190 ° | 10154 | 73 dBsm | 0.250 |
| | | 200° | 10642 | 49 dBsm | 0.015 |
| | | 210° | 11547 | 60 dBsm | 0.052 |
| | | 220° | 13054 | 48 dBsm | 0.011 |
| | | 230° | 15557 | 47 dBsm | 0.010 |
| | | 240° | 20000 | 53 dBsm | 0.018 |
| | | 250° | 29238 | 65 dBsm | 0.0673 |

## 4.2.2 Bistatic RCS and Reflection Coefficient on Incidence angle $\theta_i = 88.45°$

3D model of the Aircraft for this case is depicted in Fig. 4.13. With the help of 3D model, we can clearly observe that the bottom surface of the Aircraft body creates multiple spikes of RCS over a different Bistatic angles. We can place our receiver at ground in a more sophisticated way by analyzing the directions of those scattered signals.
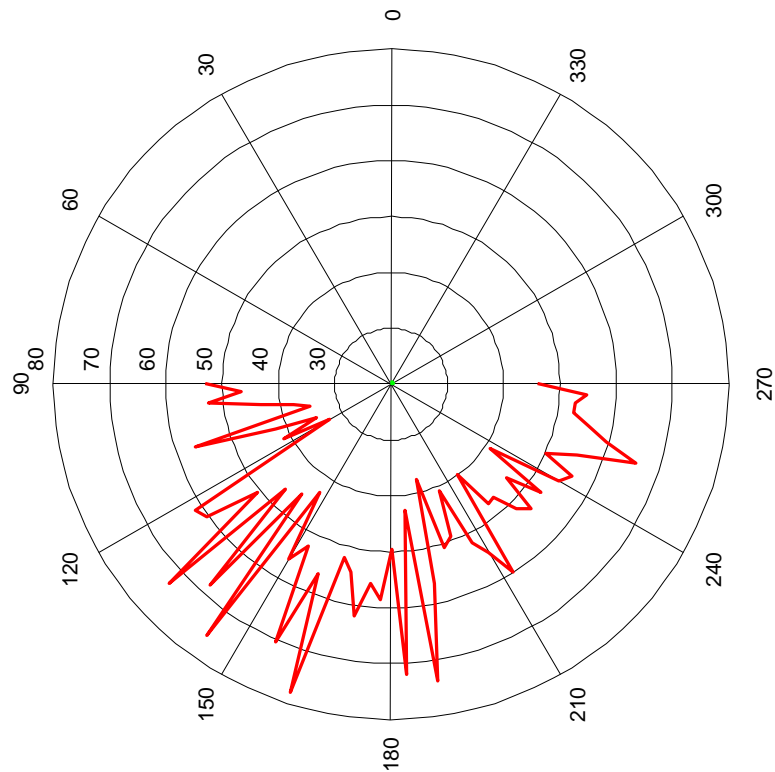
FIGURE 4.13: *3D representation of RCS calculation at incidence angle $\theta_i = 88.45°$ for the case of Ground-to-Aircraft Communication Link*

Fig. 4.14 shows the behavior of bistatic RCS for the incidence angle of 88.45 degrees in the $\phi = 0°$ plane. Observation direction or bistatic angle is varied from 90 to 270 degrees in the $\phi = 0°$ plane, using a signaling frequency of 2 GHz and the number of Taylor Series based polynomial terms set at 3. Orientation of the Aircraft is now changed according to the scenario. The major lobe at 270 degrees is the specular reflection from the bottom surface of the Aircraft body.
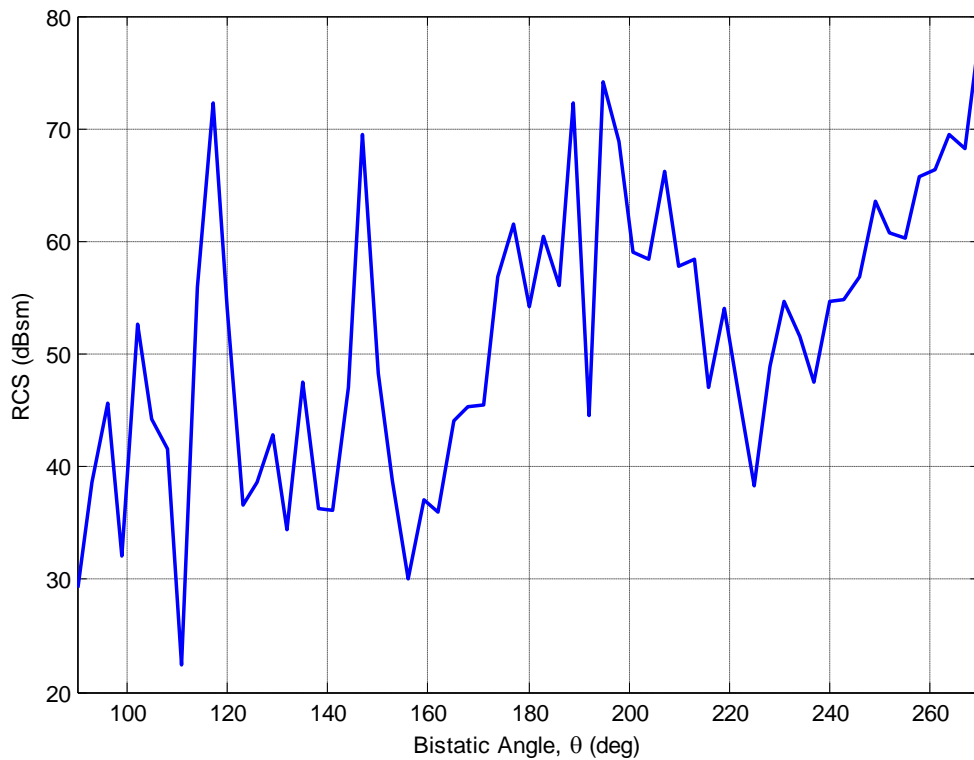
FIGURE 4.14: *RCS observation at incidence angle $\theta_i = 88.45°$ for the case of Ground-to-Aircraft Communication Link*

Other than the maximum lobe, there are multiple side lobes available as depicted in Fig. 4.14. It can be observed, that rapid change in the behavior of RCS is directly proportional to the orientation of the Aircraft and incidence angle. The lowest spike of the RCS is occur at Bistatic angle $\theta = 110°$. The leading edges of the wings and engines create multiple strong RCS spikes over a different Bistatic angles as depicted in Fig. 4.14. It can be also noticed that due to some flat surface on lower surface of Aircraft body, RCS value is increasing gradually from 237 degrees to 270 degrees. However, it can also be observed that the gain or ratio of major spike to minor spikes is increased at incidence angle of 88.45° as compared to that at incidence angle of 180°. The rapid change in the behavoir

of the RCS can also be observed in polar plot, as shown in Fig. 4.15. To know



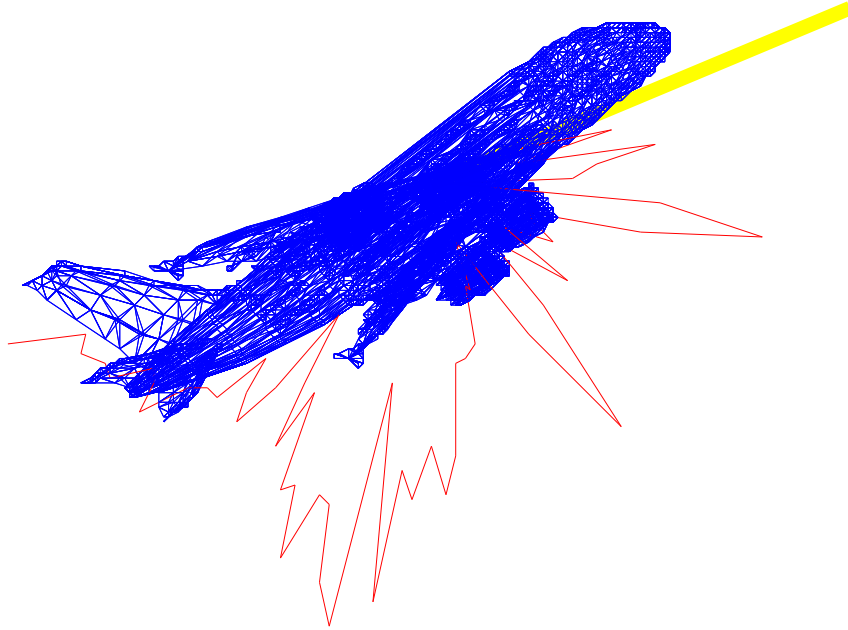FIGURE 4.15: *Polar plot representation of RCS calculation at incidence angle*
$\theta_i = 88.45°$ *for the case of Ground-to-Aircraft Communication Link*

the Reflection coefficients, RCS values from the plot in Fig. 4.14 when placed
in *Eq (1.22)* on page 17, reflection coefficients at different observation angles are
obtained. These reflection coefficients are listed in Table 4.5. It can also be
observed that the reflection coefficient at 145° is higher as compared to the others
values of reflection coefficients.

TABLE 4.5: Characterization of reflection coefficient at incidence angle $\theta_i = 88.45°$ for the case of Ground-to-Aircraft Communication Link

| Incidence angle | $d_1$(km) | Bistatic angles $(\theta)$ | $d_2$(m) | $\sigma$ | $|\Gamma|$ |
|---|---|---|---|---|---|
| 88.45° | 358 | 110 ° | 29238 | 23 dBsm | 0.0001 |
| | | 118° | 21301 | 73 dBsm | 0.0556 |
| | | 130° | 15557 | 35 dBsm | 0.0009 |
| | | 140 ° | 13054 | 37 dBsm | 0.0017 |
| | | 145 ° | 12208 | 70 dBsm | 0.0706 |
| | | 160 ° | 10642 | 37 dBsm | 0.0018 |
| | | 170° | 10154 | 45 dBsm | 0.0048 |
| | | 180° | 10000 | 55 dBsm | 0.0154 |
| | | 190° | 10154 | 46 dBsm | 0.0054 |
| | | 200° | 10642 | 59 dBsm | 0.0229 |
| | | 210° | 11547 | 57 dBsm | 0.0167 |
| | | 220° | 13054 | 50 dBsm | 0.0066 |

## 4.2.3 Bistatic RCS and Reflection Coefficient on Incidence angle $\theta_i = -88.45°$

3D model of the Aircraft is depicted in Fig. 4.16. With the help of 3D model, we can clearly observe that which part of the Aircraft body creates high or low spike of RCS. By using 3D model we can analyze the direction of the reflected signals easily. Yellow arrow represents the direction of the incidence signal while the red arrows represent the reflected or scattered signals from the Aircraft surface. Fig. 4.17 shows the behavior of bistatic RCS for the incidence angle of -88.45 degrees in the $\phi = 0°$ plane. Observation direction or bistatic angle is varied from 90 to 270 degrees in the $\phi = 0°$ plane. The Orientation of the Aircraft is changed according to Ground to Aircraft scenario. The maximum lobe at 95 degrees is the specular reflection from the bottom surface of the Aircraft. Other than the maximum
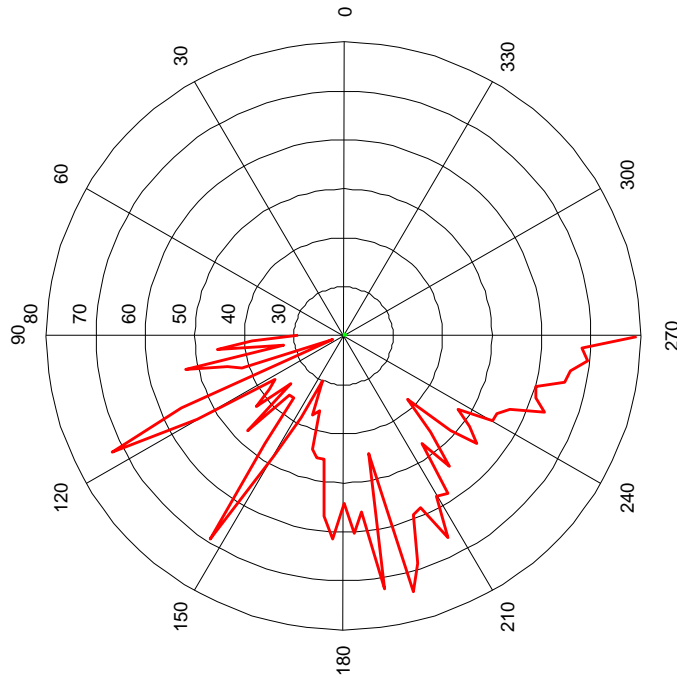
FIGURE 4.16: *3D representation of RCS calculation at incidence angle* $\theta_i =$ *−88.45° for the case of Ground-to-Aircraft Communication Link*

lobe, there are multiple side lobes available as depicted in Fig. 4.17. Side lobes occur due to the large and complex body of the Aircraft. Complex body of the Aircraft will make the reflected signals to be scattered at directions other than the desired one. Due to change in incidence angle according to our scenario, it can be observed that the behavior of the RCS is now totally changed as compared to the previous result for the incidence angle of 88.45 degrees. The leading edges of the left wing create strong RCS spike approximately at 150 degrees. Albeit different RCS spikes show up in the chart, these have significantly bring down qualities (more than 50 dB underneath the most elevated esteem), as demonstrated in the Fig. 4.17. Major lobes and changes in the behavoir of the RCS can be observed in the form of polar plot, as depicted in Fig. 4.18. Here, for $\theta$=195 degrees RCS
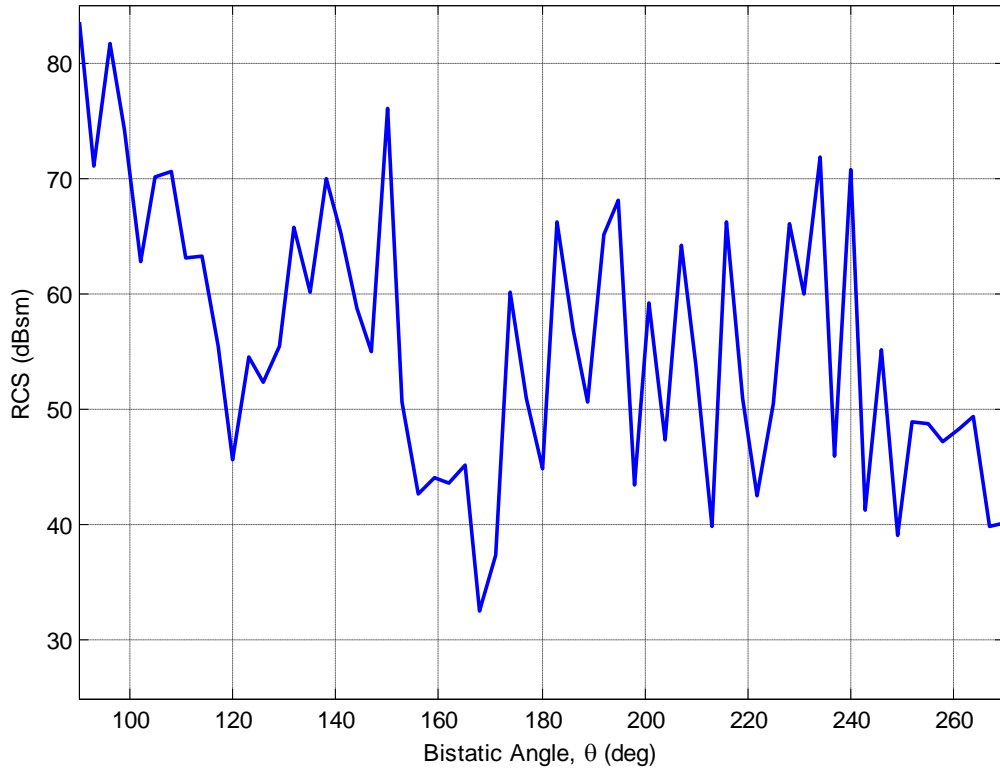
FIGURE 4.17: *RCS observation at incidence angle $\theta_i = -88.45°$ for the case of Ground-to-Aircraft Communication Link*

is the highest value and represents the major lobe of the polar plot. The value of the RCS is read in dBsm on the concentric circles in the graph. RCS values from the plot in Fig. **??** when placed in *Eq (1.22)* on page 17, reflection coefficients at different observation angles are obtained. These reflection coefficients are listed in Table 4.6. It can also be observed that the reflection coefficient at 39° is higher as compared to the others values of reflection coefficients.
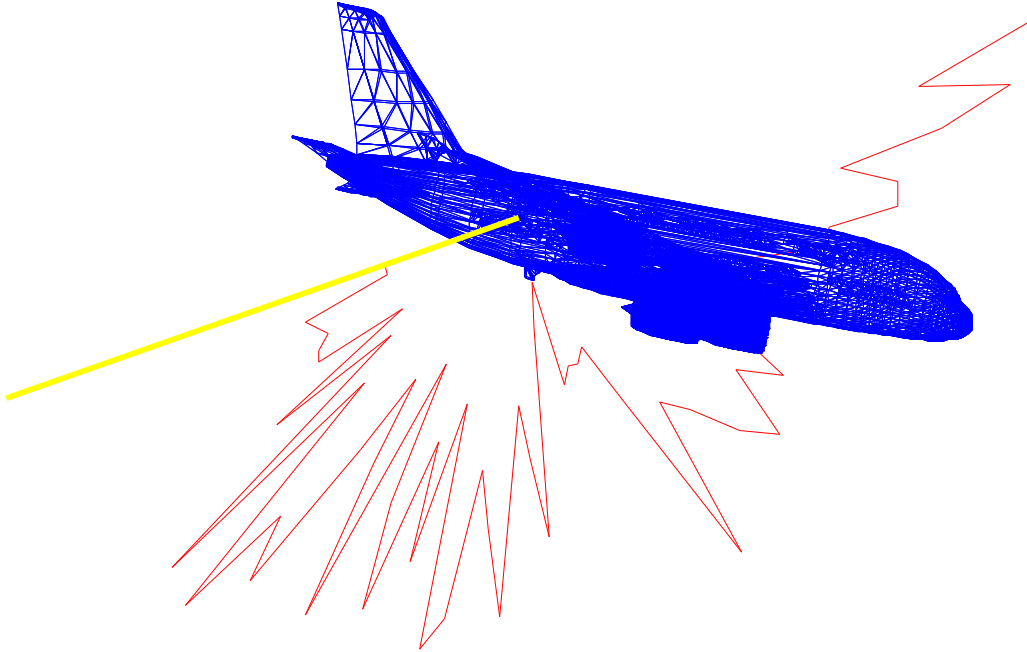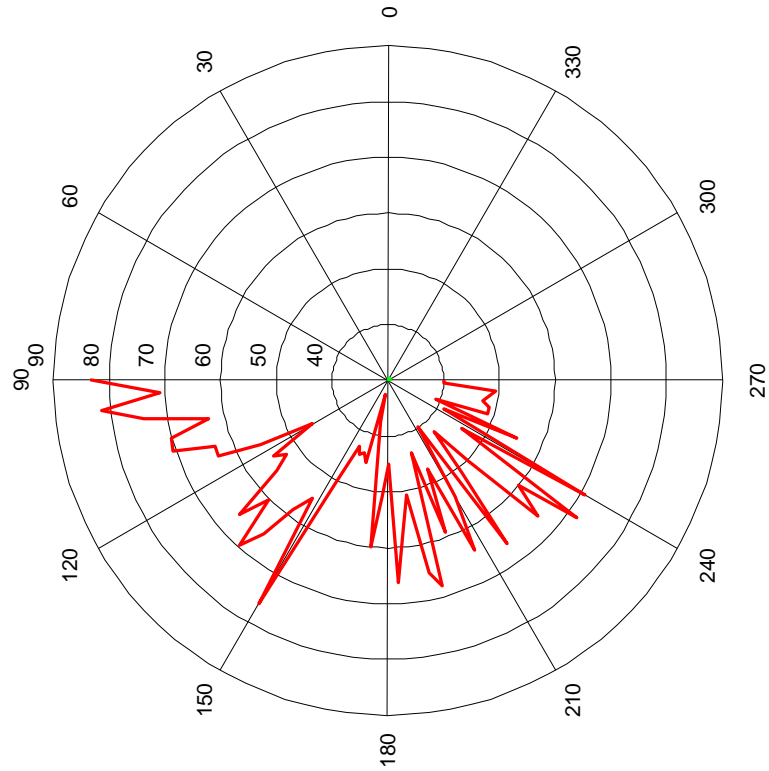
FIGURE 4.18: *Polar plot representation of RCS calculation at incidence angle*
$\theta_i = -88.45°$ *for the case of Ground-to-Aircraft Communication Link*

TABLE 4.6: Characterization of reflection coefficient at incidence angle $\theta_i = 88.45°$ for the case of Ground-to-Aircraft Communication Link

| Incidence angle | $d_1$(km) | Bistatic angles ($\theta$) | $d_2$(m) | $\sigma$ | $|\Gamma|$ |
|---|---|---|---|---|---|
| | | 110 ° | 29238 | 65 dBsm | 0.0158 |
| | | 120° | 20000 | 47 dBsm | 0.0030 |
| | | 130° | 15557 | 60 dBsm | 0.0174 |
| | | 140 ° | 13054 | 37 dBsm | 0.0467 |
| | | 150 ° | 11547 | 75 dBsm | 0.1331 |
| -88.45° | 358 | 160 ° | 10642 | 44 dBsm | 0.0041 |
| | | 170° | 10154 | 35 dBsm | 0.0015 |
| | | 180° | 10000 | 46 dBsm | 0.0055 |
| | | 190° | 10154 | 60 dBsm | 0.0270 |
| | | 200° | 10642 | 55 dBsm | 0.0145 |
| | | 210° | 11547 | 50 dBsm | 0.0075 |
| | | 220° | 13054 | 48 dBsm | 0.0052 |

# Chapter 5

## CONCLUSIONS AND FUTURE WORK

This chapter first gives a brief conclusion of the thesis in section 5.1 and then discusses future research work in section 5.2.

## 5.1   Conclusions

In this thesis, a concrete relationship has been established between RCS and reflection coefficient for the two proposed scenarios, i.e. Ground-to-Aircraft and Satellite-to-Aircraft communication links. In this study, the world's largest commercial Aircraft A380 has been selected as a target object. The well-established software tool developed by David C. Jenn, known as POFACET® has been used for the correct estimation of the RCS. POFACET® utilizes the scientific computational features of MATLAB® and its graphical-user-interface (GUI) functions to provide efficient calculation of RCS. By using official dimensions, 3D realistic model of the Aircraft A380 has been designed in AutoCAD® software. In POFACETS®, the file format of the target object needs to be in Stereo Lithography(.stl) format. The stereo Lithography file of the target Aircraft has been developed in AutoCAD®. Geometrical models of the two proposed scenarios have been used for the correct estimation of the incidence angles for the target aircraft. Angles transformation has been done for the incidence angles between POFACET® and normal mode of rotation. The obtained RCSs of A380 at different incident angles have been used to find the reflection coefficients of the target aircraft in 0° to 180° range of Bistatic(or observation angles). Various results for the different incidence angles have been simulated against bistatic angles. Direction of the reflected or scattered signals have been analyzed over a 3D model of the target Aircraft. Fluctuation on the gain or ratio of RCS major spike to minor spikes

have been studied. Factors that affect the behavior of RCS, i.e. orientation, incidence angles, and frequency have been studied and analyzed. On the basis of the obtained RCSs, Reflection coefficients of the selected object in various directions have been recorded.

## 5.2 Future works

Further work is required to investigate the behavior of RCS and reflection coefficients for different targets, incident angles and scenarios. However, new scenarios can be developed to deeply study the nature of the disturbances to Instrument-Landing-System due to Large Taxiing Aircraft. In future, investigation is needed for Scattering Distortion System Analysis of RCS and Radar Propagation Near Offshore Wind Farms.

# REFERENCES

[1] H. Singh and R.M. Jha. *Active Radar Cross Section Reduction.* Cambridge University Press, 2015.

[2] I.P.E.S.S. Committee, Institute of Electrical, and Electronics Engineers. *IEEE Standard[s].* Number no. 686. Institute of Electrical and Electronics Engineers, 1990.

[3] RTO EDUCATIONAL NOTES EN-SET. Knowledge-based radar signal and data processing. 2007.

[4] *Introduction to Radar Systems.* Tata McGraw Hill, 2001.

[5] Merrill I Skolnik. An analysis of bistatic radar. *Aerospace and Navigational Electronics, IRE Transactions on*, (1):19–27, 1961.

[6] M. Jankiraman, N.J. Willis, and H. Griffiths. *Design of Multi-Frequency CW Radars.* Electromagnetics and Radar. Institution of Engineering and Technology, 2007.

[7] E.F. Knott, J.F. Schaeffer, and M.T. Tulley. *Radar Cross Section.* SciTech (New York, N.Y). Institution of Engineering and Technology, 2004.

[8] Elmo E Garrido Jr. Graphical user interface for a physical optics radar cross section prediction code. Technical report, DTIC Document, 2000.

[9] M.C. Budge and S.R. German. *Basic Radar Analysis:.* Artech House Radar Library. Artech House Publishers, 2015.

[10] E.F. Knott. *Radar Cross Section Measurements.* Springer US, 2012.

[11] D. Curtis Schleher. *Electronic Warfare in the Information Age.* Artech House, Inc., Norwood, MA, USA, 1st edition, 1999.

[12] W.L. Stutzman. *Polarization in Electromagnetic Systems.* Artech House antenna library. Artech House, 1993.

[13] D. F. Bacon. Introduction to diffraction, reflection and scattering. In M. P. M. Hall, L. W. Barclay, and M. T. Hewitt, editors, *Propagation of Radiowaves*, page 60, 1996.

[14] Theodore S Rappaport. Wireless communications–principles and practice, (the book end). *Microwave Journal*, 45(12):128–129, 2002.

[15] Timothy Pratt and Charles W Bostian. *Satellite communications.* John Wiley & Sons, 1986.

[16] Orlando Landron, Martin J Feuerstein, and Theodore S Rappaport. In situ microwave reflection coefficient measurements for smooth and rough exterior wall surfaces. In *Vehicular Technology Conference, 1993., 43rd IEEE*, pages 77–80. IEEE, 1993.

[17] Orlando Landron, Martin J Feuerstein, and Theodore S Rappaport. A comparison of theoretical and empirical reflection coefficients for typical exterior wall surfaces in a mobile radio environment. *Antennas and Propagation, IEEE Transactions on*, 44(3):341–351, 1996.

[18] B.R. Mahafza. *Introduction to Radar Analysis*. Advances in Applied Mathematics Series. Taylor & Francis, 1998.

[19] Merrill Ivan Skolnik. Radar handbook. 1970.

[20] GT Ruck and CK Krichbaum. Radar cross section handbook. supplement, part 1. theoretical techniques for diffraction bodies. Technical report, DTIC Document, 1968.

[21] Björn Persson and Martin Norsell. On modeling rcs of aircraft for flight simulation. *Antennas and Propagation Magazine, IEEE*, 56(4):34–43, 2014.

[22] SK Wong, E Riseborough, G Duff, and KK Chan. Radar cross-section measurements of a full-scale aircraft duct/engine structure. *IEEE transactions on antennas and propagation*, 54(8):2436–2441, 2006.

[23] Wei-Dong Li, Jun-Xia Miao, Jun Hu, Zhe Song, and Hou-Xing Zhou. An improved cubic polynomial method for interpolating/extrapolating mom matrices over a frequency band. *Progress In Electromagnetics Research*, 117:267–281, 2011.

[24] Wei-Dong Li, Hou-Xing Zhou, Jun Hu, Zhe Song, and Wei Hong. Accuracy improvement of cubic polynomial inter/extrapolation of mom matrices by optimizing frequency samples. *Antennas and Wireless Propagation Letters, IEEE*, 10:888–891, 2011.

[25] Jon David Wilson. Probability of detecting aircraft targets. *Aerospace and Electronic Systems, IEEE Transactions on*, (6):757–761, 1972.

[26] Robert Geise, Achim Enders, Helge Vahle, and Harald Spieker. Scaled measurements of instrument-landing-system disturbances due to large taxiing aircraft. *Electromagnetic Compatibility, IEEE Transactions on*, 50(3):485–490, 2008.

[27] Hiroshi Shirai, Takaaki Ishikawa, and Yuji Watanabe. A study of radar cross-section measurements in an anechoic chamber. *Electrical Engineering in Japan*, 123(1):8–14, 1998.

[28] Kuizhi Yue, Yong Gao, Guanxiong Li, and Dazhao Yu. Conceptual design and rcs performance research of shipborne early warning aircraft. *Systems Engineering and Electronics, Journal of*, 25(6):968–976, 2014.

[29] Funda Ergun Yardim and Nursel Akcam. Estimation of radar cross-section in rayleigh, mie, and optical regions by the 2-d-fdtd simulation. *Antennas and Propagation, IEEE Transactions on*, 62(11):5782–5789, 2014.

[30] Charlotte Corbel, Christophe Bourlier, Nicolas Pinel, and Janic Chauveau. Rough surface rcs measurements and simulations using the physical optics approximation. *Antennas and Propagation, IEEE Transactions on*, 61(10):5155–5165, 2013.

[31] Isamu Matsunami, Ryosuke Nakamura, and Akihiro Kajiwara. Rcs measurements for vehicles and pedestrian at 26 and 79ghz. In *Signal Processing and Communication Systems (ICSPCS), 2012 6th International Conference on*, pages 1–4. IEEE, 2012.

[32] Ayhan Altintas and Aslihan Celik. Large flat plate models in the physical optics method for rcs calculations. In *Mathematical Methods in Electromagnetic Theory, 2004. 10th International Conference on*, pages 586–588. IEEE, 2004.

[33] PA Lees and MR Davies. Computer prediction of rcs for military targets. In *Radar and Signal Processing, IEE Proceedings F*, volume 137, pages 229–236. IET, 1990.

[34] Naval Postgraduate School Monterey CA and F. Chatzigeorgiadis. *Development of Code for a Physical Optics Radar Cross Section Prediction and Analysis Application*. Storming Media, 2004.

[35] D.C. Jenn. *Radar and Laser Cross Section Engineering*. AIAA education series. American Institute of Aeronautics and Astronautics, 1995.

[36] Dr. David C. Jenn. POFACETS. `http://faculty.nps.edu/jenn/#_Matlab_Software`, 2004. [Online; accessed 21-June-2016].

[37] Filippos Chatzigeorgiadis and David C Jenn. A matlab physical-optics rcs prediction code. *IEEE Antennas and Propagation Magazine*, 46(4):137–139, 2004.

[38] Elmo E Garrido Jr and David C Jenn. A matlab physical optics rcs prediction code. 2000.

[39] Syed Junaid Nawaz, Noor M Khan, Moazzam Islam Tiwana, Najmul Hassan, and Syed Ismail Shah. Airborne internet access through submarine optical fiber cables. *IEEE Transactions on Aerospace and Electronic Systems*, 51(1):167–177, 2015.